HIGHLIGHTS

- Cardanols are natural occurring alkylphenols byproducts of cashew nut processing
- Hydrogenated cardanol derivatives (HC) were co-micellized with Triton X-100
- CMC, microviscosity, polarity, aggregation number of co-micelles were obtained
- HC in micelles demonstrated radical-trapping
- HC in micelles demonstrated protective activity toward peroxidation of PEG tails

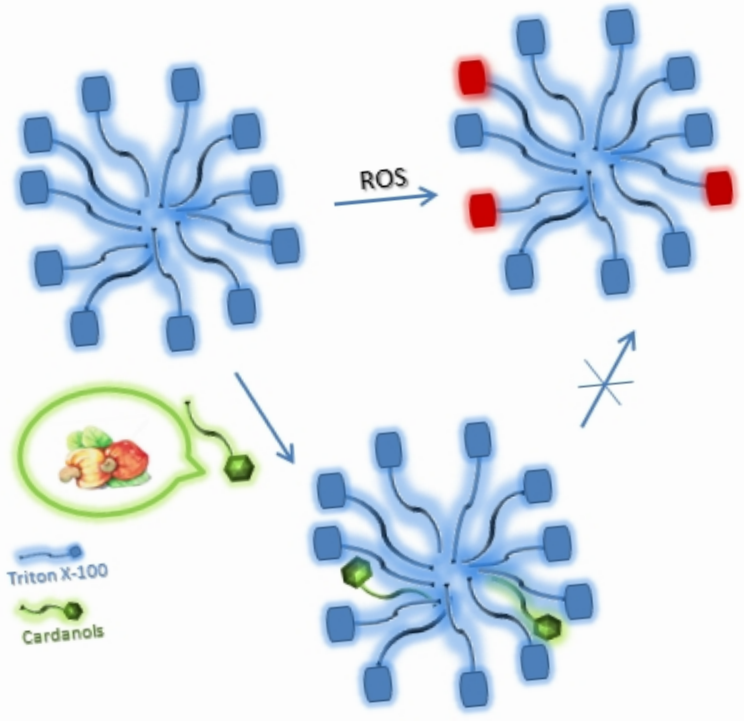
ROS
Triton X-100
Cardanols

Cardanol-like co-surfactants solubilized in pegylated micelles keep their antioxidant activity and preserve polyethylene glycol chains from oxidation

Antonella Fontana,[a*] Susanna Guernelli,[b*] Antonello Di Crescenzo,[a] Pietro Di Profio,[a] Francesco Palomba,[b] Lucia De Crescentini,[c] Andrea Baschieri[b] and Riccardo Amorati[b]

[a]*Dipartimento di Farmacia, Università "G. d'Annunzio", Via dei Vestini 31, 66100 Chieti, Italy*

[b]*Dipartimento di Chimica "G. Ciamician", Università degli Studi di Bologna, Via S. Giacomo 11 and Via Selmi 2, 40126 Bologna, Italy*

[c]*Dipartimento di Scienze Biomolecolari, Università di Urbino "Carlo Bo", Via Maggetti 24, 60129 Urbino, Italy*

Corresponding Authors: fontana@unich.it (AF) and susanna.guernelli@unibo.it (SG)

KEYWORDS: Cardanol derivatives; antioxidant activity; micelles; polyethylene glycol-chained surfactants; polyethylene glycol oxidation

Abstract. Pegylated (PEG) surfactants ~~olyethylene glycols (PEG)~~ are widely used ~~surfactants~~ for material and biomedical applications. Their use, however, is limited by the radical-mediated oxidation of the OCH_2 moieties by atmospheric oxygen, that produces unwanted and toxic products such as hydroperoxides. We show herein that cardanols, natural alkylphenols byproducts of cashew nut processing, are able to form stable co-micellar systems with a model PEG-

containing surfactant (Triton X-100, i.e. p-*tert*-octylphenoxy polyethylene-glycol ether) and display antioxidant activity toward PEG degradation by O_2. The cardanols investigated were 6-*tert*-butyl-3-pentadecylphenol and 4-hydroxy-6-*tert*-butyl-3-pentadecylphenol derivatives. The ability of cardanols to form co-micelles with Triton X-100 was investigated by determining the CMC, the microviscosity, the polarity and the aggregation number of the aggregates. The antioxidant activity of cardanol derivatives in dispersed systems of Triton X-100 was evaluated by studying the reaction with DPPH radical and the protecting activity toward the peroxidation of the polyethylene-glycol tails. The obtained activity of cardanol derivatives was similar or better than that of commercial synthetic antioxidants BHT (2,6-di-*tert*-butyl-4-methylphenol) and DTBQ (2,5-di-*tert*-butylhydroquinone), taken as reference, under the same conditions. This study enlightens the ability of hydrogenated cardanol derivatives to act as radical-trapping agents and/or as protective co-surfactants toward the oxidative degradation PEG-coated nanoaggregates used in food and drug science.

1. Introduction

Polyethylene glycol(PEG)-chained surfactants are popular means for the solubilization of water insoluble molecules that have recently received great attention for the preparation of PEG-coated nanoobjects, usable as carrier systems in pharmaceutical applications [1-3] and in the field of food packaging and food safety [4]. PEG serves as a stealth corona to avoid capture by macrophage and favors circulation of nanoparticles in the blood stream [5], and it can form solid hydrophilic matrixes easy to hydrate and capable to form gels [6]. However, being a poly-ether, in the presence of oxygen, PEG undergoes radical-mediated oxidation which generates unstable hydroperoxides, which then react further, leading ultimately to the cleavage of C-O bonds and consequent shortening of the PEG chain and formation of reactive aldehydes [7, 8]. This drawback limits the

applications of PEG-based surfactants [9] and requires the addition of antioxidants to reduce the problem [10].

The use of antioxidant agents from natural sources, such as plant-derived compounds, has received increasing interest in the recent literature as a means to replace synthetic phenols both for sustainability and toxicity reasons [11-15].

Cardanol is considered one of the most interesting examples of sustainable plant-derived raw material. It is the main constituent of Cashew Nut Shell Liquid (CNSL), a by-product obtained from cashew nut (*Anacardium occidentale L.*), whose final precise composition - depending on the extraction method - is mainly based on cardanol, cardol, anacardic acid and methylcardanol, with different unsaturation degrees on the alkyl sidechain [16-18]. The antioxidant activity of some cardanol derivatives, compared with that of analogous commercial products, has been studied by some of us and the data obtained demonstrated that these compounds represent a convenient alternative to synthetic antioxidants [19-21]. Very recently, epoxidized cardanol have been investigated for their antioxidative properties for vegetable oils and biodiesel [22], whereas cardanol-derived arylamines demonstrated superior antioxidant properties and thermal-oxidation stability [23]. These results are particularly relevant because cardanol and its hydrogenated derivatives ~~is~~are biocompatible, biodegradable [24 - 26] and non-persistent in the environment [~~25~~27].

In a previous paper we have proved that hydrogenated cardanol behaves as a co-surfactant of Triton X-100 in a percentage as high as 10% mole ratio and, therefore, it can be used as such in order to promote sustainability and renewability of commercial amphiphiles [~~26~~28].

In the wake of these considerations here we have investigated the antioxidant performance toward the peroxidation of polyethylene-glycol (PEG) tails and toward the stable 2,2-diphenyl-1-picrylhydrazyl (DPPH•) free radical [~~27~~29, ~~28~~30] of hydrogenated cardanol derivatives (6-*tert*-

butyl cardanol, TBC, and 6-*tert*-butyl-4-hydroxy cardanol TB(OH)C), see Figure 1, when they are incorporated in micelles of Triton X-100.

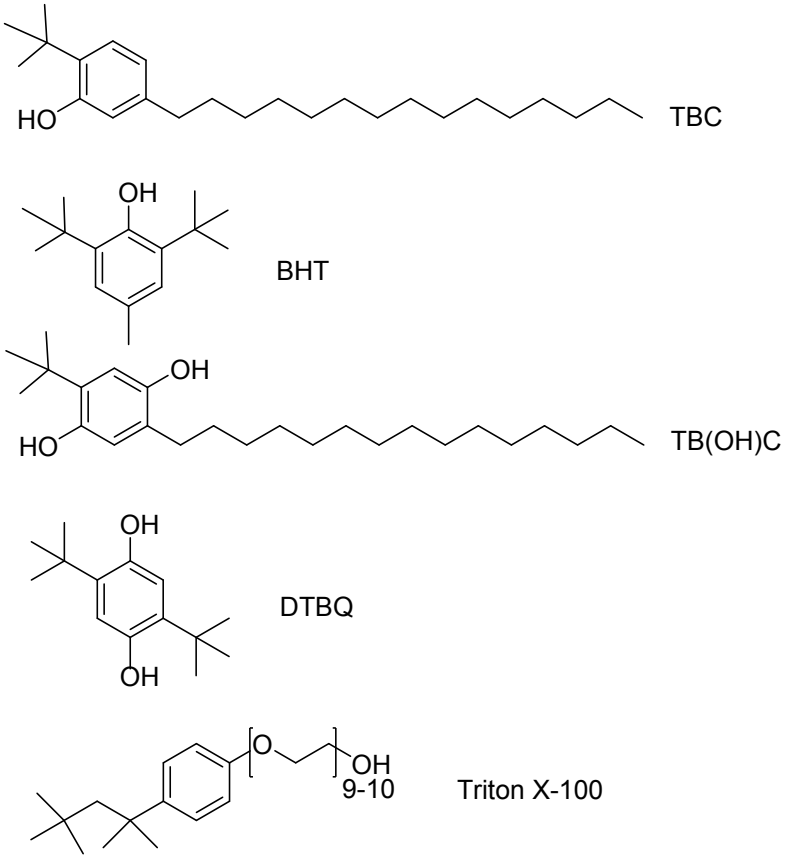

Fig. 1. Chemical structure of hydrogenated cardanol derivatives (TBC and TB(OH)C), the reference antioxidants BHT and DTBQ, and Triton X-100 surfactant.

TBC and TB(OH)C where chosen because they showed a better antioxidant activity compared to cardanol in ~~homogeneous~~ organic solvents [19 - 21]. The aim of the present study is to investigate in detail the mixed cardanol derivative/Triton X-100 micelles. In particular, the localization of antioxidants was studied through surface tension measurements of CMC and spectrofluorimetric evidences of microviscosity, polarity and aggregation number whereas spectrophotometric evidences allowed to investigate the arrangement of radicals in the micelles. All these data were

used to compare the effect of the different cardanol derivatives on micelles features and to interpret both the obtained DPPH• scavenging data and inhibition of Triton X-100 peroxidation.

2. Materials and Methods

2.1. Materials

Triton X-100 (peroxide free, as assessed by QUANTOFIX® Peroxide test strip), pyrene (99%), BHT (2,6-di-*tert*-butyl-4-methylphenol), DTBQ (2,5-di-*tert*-butylhydroquinone), 2,2′-Azobis(2-methylpropionamidine) dihydrochloride (AAPH), diphenylpicrylhydrazyl (DPPH•) radical, 2,2,5,7,8-pentamethyl-6-chromanol (PMHC) and solvents of analytical grade were purchased from Sigma-Aldrich and used without further purification. Water was HPLC grade. Samples of 6-*tert*-butyl hydrogenated cardanol [~~29~~31] and 6-*tert*-butyl-4-hydroxy hydrogenated cardanol [~~30~~32], having a saturated alkyl chain, were kindly provided by Prof. Attanasi (University of Urbino). NMR spectra, performed in order to confirm the degree of purity of TBC and TB(OH)C, are reported in the Electronic Supplementary Information, section S1.

Aqueous dispersions were obtained by solubilizing the investigated antioxidant or cardanol derivative in aqueous solutions of Triton X-100 of the elected concentration.

2.2. Tensiometric analyses

Surface tension measurements were performed with a SensaDyne tensiometer QC6000 via the bubble pressure method. Triton X-100 solutions at different concentrations were obtained by diluting a concentrated mother solution to the elected value. Readings, recorded at room temperature, were taken after thorough mixing. The accuracy of measurements was within ±0.1 dyne cm^{-1}. Surface tension values (dyne cm^{-1}) were plotted against the decimal logarithm of the molar concentration of the Triton X-100 in order to evaluate the relevant CMC. The investigated

concentrations of Triton X-100 were 2.00×10^{-5} - 4.00×10^{-3} M. The obtained CMC is the mean value of at least two different measurements.

2.3. Aggregation number

The aggregation number was determined by exploiting the fluorescence quenching method [~~31~~33] and using pyrene as the fluorescent molecule and N,N-dibutylaniline (DBA) as the quencher [~~26~~28].

An appropriate volume of pyrene stock solution in ethanol was added to a cuvette containing the 2.00×10^{-2} M Triton X-100 aqueous solutions. The concentration of Triton X-100 was chosen in order to reduce the fraction of micelles with more than one pyrene molecule.

After evaporation of the ethanol, DBA, dissolved in dioxane, was added to the cuvette in order to obtain a range of quencher concentrations of 5–100 μM while keeping the concentrations of pyrene and the surfactant constant. Pyrene was excited at λ 335 nm and the emission intensity (I_0) was monitored at λ 376 nm and λ 395 nm. If the micelles are assumed to be monodisperse, the relative intensity of fluorescence emission (I) is given by the following equation: $\ln(I_0/I) = N[Q]/(C - CMC)$ where I_0 is the fluorescence intensity in the absence of quencher, [C] is the total surfactant concentration, [Q] is the quencher concentration and N is the surfactant aggregation number.

2.4. Microviscosity and micropolarity

The microviscosity and micropolarity of the Triton X-100 micelles (2.00×10^{-3} M) have been determined fluorimetrically using pyrene as the fluorescent probe [~~32~~34, ~~33~~35]. Fluorescence emission spectra were recorded using an excitation wavelength of 335 nm. The fluorescence intensity ratio, I_E/I_M, was used to determine the microviscosity, where I_E, the emission at λ 473 nm, is the intensity of the excimer and I_M, the emission at λ 395 nm, is the intensity of the monomer. The micropolarity was measured by the intensity ratio of the first and the third band of

the pyrene emission spectrum, I_1/I_3, where I_1 is the emission at λ 374 nm and I_3 is the emission at λ 385 nm.

2.5. Spectrophotometric determination of the localization of DPPH• radical in the micelles

The micellar localization of the scavenger DPPH• was provided by monitoring the position of its mixed valence band centered at about λ 520 nm. This band can be used as a solvatochromic tool as it can shift to higher wavelengths in the presence of an aggregation process promoted in aqueous media. Experimentally, a concentrated solution of DPPH• was prepared in methanol (1.0×10^{-3} mol/L). This solution was used as a stock solution for the preparation of sample with different dispersants (acetonitrile, methanol, water/methanol 4:1, Triton X-100 1.0×10^{-3} M and 1.00×10^{-5} M), diluting few microliters directly in quartz cuvette with a final DPPH• concentration of 1.0×10^{-6} M. After that, the spectra were recorder with a Cary UV 300 spectrophotometer.

2.6. Determination of DPPH• scavenging

The reactivity of micellized antioxidants toward the DPPH• radical was assessed by measuring the disappearance of the DPPH• absorption band at λ 517 nm after injecting the proper amount of methanolic DPPH• solution (final concentration $2.0 – 15.0 \times 10^{-5}$ M) into a quartz cuvette containing micelles of Triton X-100 (1.29×10^{-3} M) and the antioxidant (1.29×10^{-4} M) [~~34~~36]. The stoichiometry of the reaction (i.e., number of radicals quenched by each antioxidant) was determined by using a slight excess of DPPH•, whereas the rate constant was obtained by using antioxidants in large excess. Reaction rates constants were obtained from the absorption decrease by fitting the experimental data with a kinetic simulator software (Gepasi) [~~35~~37] by using well assessed reaction schemes (see Electronic Supplementary Information) [~~36~~38]. The spectra were recorder with a Jasco V-550 spectrophotometer.

2.7. Inhibition of Triton X-100 peroxidation

Formation of hydroperoxides during Triton X-100 autoxidation initiated by the water-soluble azo-initiator 2,2′-Azobis(2-methylpropionamidine) dihydrochloride (AAPH) was qualitatively evaluated with the ferrous xylenol orange test (QUANTOFIX® Peroxide test strip). The extent of Triton X-100 peroxidation was quantitatively evaluated by measuring the O_2 consumption by a differential oxygen uptake apparatus build in our laboratory and based on a Validyne DP 15 differential pressure transducer [~~37~~39, ~~38~~40]. Triton X-100 peroxidation was initiated by AAPH at 30 °C and the O_2 uptake was measured in the absence and in the presence of the co-micellized antioxidants. In a typical experiment, an air-saturated Triton X-100 (13 mM), containing AAPH (5 mM) was equilibrated with a reference solution containing only water. After equilibration, and when a constant O_2 consumption was reached, a small amount of a concentrated solution of the antioxidant (final concentration 1.3 mM) was injected in the sample flask. The oxygen consumption in the sample was measured after the calibration of the apparatus from the differential pressure recorded with time between the two channels. Initiation rates, Ri, were determined in the preliminary experiments by the inhibitor method using 2,2,5,7,8-pentamethyl-6-chromanol (PMHC) as a reference.

3. Results and Discussion

3.1. Arrangement of guests in the micelles

In order to gauge the effect of the guests (hydrogenated cardanol derivatives and commercial antioxidants) on the surfactant features as well as the position of the guests into the micelles we evaluated the critical micelle concentration (CMC), the aggregation number, the micellar dimensions, the microviscosity and the polarity of the micellar systems. CMC data (Table 1 and Electronic Supplementary Information) highlight an increase of CMC upon addition of the guests. The CMC is two and three times higher than that of Triton X-100 for DTBQ and BHT, respectively, whereas the increase of CMC is less marked and approximately related to the increase

of guests molecular weight and/or steric hindrance when cardanol guests are considered. The observed increase of CMC values in the presence of synthetic antioxidants is therefore indicative of a more difficult micellization. Since it is generally accepted that solubilization of guests in the shell region increases the CMC [~~39~~41], it is likely that these guests solubilize in the polyoxyethylene shell of the micelles. It is important to stress at this point that previous studies [~~40~~42, ~~41~~43] referring to a prevailing residence of BHT in the micellar core of micelles did consider a concentration ratio of 5×10^{-4} and 5×10^{-2} for BHT/Triton X-100 and BHT/POE(23) lauryl ether, respectively. In the present case the concentration of BHT is therefore 200 and 2 times higher than the one used in those reports and a BHT partition in both regions in the present study is very likely. Indeed, Torres et al. [~~42~~44] demonstrated that very hydrophobic molecules such as fullerene C_{60} affect the arrangement of Triton X-100 molecules around themselves by pushing the 1,1,3,3-tetramethylbutyl moiety towards the outer side of the aggregate. A similar arrangement would equally explain our polarity and viscosity data as well as the capability of radicals to encounter the partially core-confined BHT (see below).

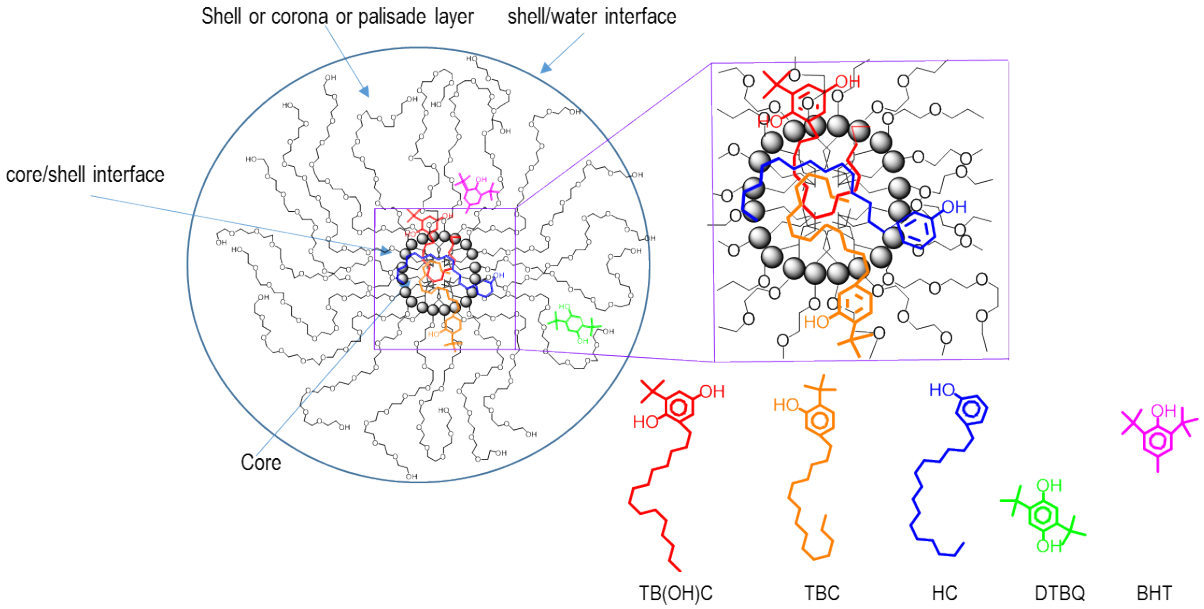

Figure 2. Distribution scheme of guests in Triton X-100 micelles.

Very interestingly, the dimensions of the micelles, determined by dynamic laser light scattering techniques, do not change on addition of guests (Table 1 and Electronic Supplementary Information). This is indicative of the fact that guests do not solubilize simply in the core of the micelle. Likely, the cardanol derivatives localize at the core/shell interface with long alkyl chains anchored to the micellar core and polar head exposed in the shell layer (i.e. corona region) (See Figure 2). This arrangement ensures the maintenance of the micelle dimensions due to a compensation effect. Moreover, depending on the hydrophilicity of the head group and the capacity of the guests to interact via hydrogen bonding, the guest will be more or less exposed towards the shell layer (see below). On the other hand DTBQ and BHT, that lack the anchoring chain and therefore are more hydrophilic with respect to cardanol derivatives (i.e. log P calculated using Advanced Chemistry Development (ACD/Labs) are 5.17±0.34 for BHT, 4.16±0.32 for DTBQ, 9.18±0.19 for HC, 10.79±0.22 for TBC and 9.66±0.30 for TB(OH)C) can spread further into the shell layer where they can establish hydrogen bonding with the polyoxyethylene chains. The fact that the solubilization of these guests do not change the size of micelles agrees with evidences of Dharaiya and Bahadur [~~43~~45] that demonstrated that no size variations were obtained for inclusion of less than 10% of phenols in Triton X-100 micelles. Indeed, Patel et al. [~~44~~46] observed an increase of dimensions and aggregation number of Triton X-100 micelles on addition of parabens and gallates but they investigated concentrations of Triton X-100 from 4 to 80 times higher than those used in the present study and concentrations of antioxidants higher than 10 mol%.

Table 1. CMC, Aggregation number (N_{Agg}), size, microviscosity and micropolarity of the investigated micellar systems in water.

Antioxidant guest	CMC (mM)	Size (nm)	N_{Agg}	Relative viscosity	Polarity
Pure Triton X-100	0.56±0.08[a]	6.7 ± 0.2 [a]	106 ± 2 [a]	1	1.29±0.07
HC 10%	0.62±0.08 [a]	10.0 ± 0.1 [a]	99 ± 1 [a]	1.3	1.21± 0.01
TBC 10%	0.79±0.19	8.0 ± 1.0	81 ± 1	1.5	1.3± 0.01
BHT 10%	1.50±0.45	7.0 ± 1.0	87 ± 3	1.4	1.22±0.01
TB(OH)C 10%	0.98±0.22	8.0 ± 1.0	51 ± 4	1.5	1.14±0.03
DTBQ 10%	1.01±0.09	7.0 ± 1.0	36 ± 2	1.5	1.13±0.04

[a] Reference ~~26~~28, values obtained by using the surface tension method.

We choose to evaluate the micropolarity and the microviscosity of the micelles with pyrene. Pyrene is known to locate on a time average in the inner shell layer of the micelle [~~45~~47, ~~46~~48] and therefore should be ideal for discriminating the effect of the investigated guests on Triton X-100 micelles. By considering the well-known Pyrene Scale [~~47~~49], it appears that, in pure Triton X-100 and TBC/Triton X-100 micelles, pyrene molecules sense a polar environment similar to pure tetrahydrofuran (ε = 7.6) or methanol (ε = 32.7). Instead in the presence of cardanol, BHT and even more TB(OH)C and DTBQ, the pyrene molecules feel a less polar environment (lower values of I_1/I_3), similar to ethyl ether (ε = 4.3) or ethanol (ε = 24.5).

Guests containing two hydroxyl groups per molecule, i.e. TB(OH)C and DTBQ, are more prone to establish hydrogen bonds with the neighboring polyoxyethylene chains and displace a larger number of water molecules from the shell region thus decreasing the polarity experienced by pyrene [~~43~~45, ~~48~~50]. In the presence of BHT, pyrene feels a less hydrophilic environment due either to the presence of the guest itself in the shell region or to the above mentioned BHT-induced different arrangement [~~42~~44] of Triton X-100 molecules in the micelles. On the other hand, due to

its high log P value, TBC, extends barely in the shell region and the presence of the *tert*-butyl group in close proximity with the polar hydroxyl head group at the core/shell interface hampers hydrogen bond formation with the polyoxyethylene chains and results in a shell region that is as hydrated as in pure Triton X-100.

The microviscosity is similarly spectrofluorimetrically measured [~~49~~51] by exploiting the tendency of pyrene to solubilize in the micelle and form excimers. This is an indirect measurement of microviscosity and every event that slows down the excimer formation is translated into a microviscosity increase, or a corresponding "microfluidity" decrease, of the shell region of the micelle (see Electronic Supplementary Information) [~~50~~52]. In the present systems, all the guests induce a decrease of excimer formation. The shell layer of the guest containing micelles is altered with respect to that of pure Triton X-100 for the presence of sterically hindered guests establishing hydrogen bonds with the polyoxyethylene chains. The measured decrease of micellar microfluidity (Table 1) agrees with the demonstrated increase of the relative viscosity of Triton X-100 solution in the presence of α-naphthol, p-cresol and phenol [~~43~~45, ~~51~~53]. The decrease of microfluidity of the shell layer, particularly evident for TB(OH)C and DTBQ enriched Triton X-100 micelles, may be related to the network of hydrogen bonds established among hydroxyl phenolic groups and polyoxyethylene chains. Interestingly, TBC decreases the fluidity of Triton X-100 micelles in which it is solubilized but does not alter the corresponding polarity. As mentioned above, the head group of TBC is less prone to extend towards the shell region with respect to the other guests and establish hydrogen bonds. Despite the unmodified hydration with respect to pure Triton X-100 micelles, the presence of *tert*-butyl groups at the core/shell interface of TBC/Triton X-100 micelles affects the mobility of pyrene and the related microfluidity of the shell region.

The addition of guests causes the reduction of the aggregation number, that appears to be approximately inversely related to the corresponding CMC, i.e. the aggregation number is 99±1

for HC, 81±1 for TBC and 51±4 for TB(OH)C (hydrogenated cardanol derivatives) and 87±3 and 36±2 for BHT and DTBQ, respectively (Table 1 and Electronic Supplementary Information). A reduction of the aggregation number on increasing the steric hindrance in the two series of guests can be noticed in agreement with an increase of packing of the head groups at the core/shell interface [~~52~~54]. The particularly low aggregation number highlighted for the dihydroxyl-substituted guests, i.e. TB(OH)C and DTBQ, can be a consequence of the extended network of hydrogen bonds established among the hydroxyl groups of the guests and the polyoxyethylene chains. This organization can induce a transition of the aggregation mode from a micellar aggregation directed by the alkyl chain packing in the core to an aggregation directed by the head group. A similar change has been evidenced for long PEG chains [~~53~~55] and caused the halving of the aggregation number on doubling the PEG length of the surfactant.

We measured also the CMC of Triton X-100 added with 10% DPPH. The relevant CMC $(1.47\pm0.41)\times10^{-3}$ M is ca. 2.5 times higher than that of pure Triton X-100, thus confirming the prevailing solubilization of DPPH• in the micellar corona region in strict contact with the antioxidative guests [~~39~~41]. Unluckily, it was not possible to perform viscosity and polarity measurements, because DPPH• demonstrated to significantly quench pyrene molecules (see Electronic Supplementary Information, Figure ~~S15~~S19).

3.2. Antioxidant activity

The radical trapping ability of the micellized TBC and TB(OH)C was assessed by studying the reaction with the 2,2-diphenyl-1-picrylhydrazyl radical (DPPH•), which is commonly used as preliminary test for the estimation of the antioxidant activity [~~34~~36]. In the presence of reducing molecules, the purple DPPH• radical is reduced to the yellow hydrazine through a formal H atom transfer reaction [~~54~~56]. As reference antioxidants, the commercial inhibitors DTBQ and BHT were also investigated. Reactions were followed by UV-vis spectroscopy by measuring the

decrease of the absorption maximum of DPPH• as a function of time after mixing a small volume of a methanol solution of DPPH• with Triton X-100 co-micellized with the tested antioxidants. For each co-micellized antioxidant, two sets of experiments were performed, with DPPH• in excess or as limiting reagent (with respect to the antioxidant), to determine with improved accuracy the stoichiometries and the reaction rates, respectively. Rate constants were obtained from the absorption decrease by fitting the experimental data with a kinetic simulator software (Gepasi) [~~35~~37, ~~36~~38]. The reaction mechanism is exemplified in Figure 3. In the case of compounds having the hydroquinone moiety, the reaction of the semiquinone radical with oxygen to form HOO• had to be considered to explain the low stoichiometry of radical trapping (see Figure 3B) [~~55~~57]. The results are reported in Table 2, together with the rate constant for the reaction with alkylperoxyl radicals measured in ~~homogeneous~~ organic solution for comparison purposes [19]. Figure 4 reports, as an example, the kinetics of DPPH• radicals reacting with TBC and TB(OH)C in the presence of Triton X-100 micelles.

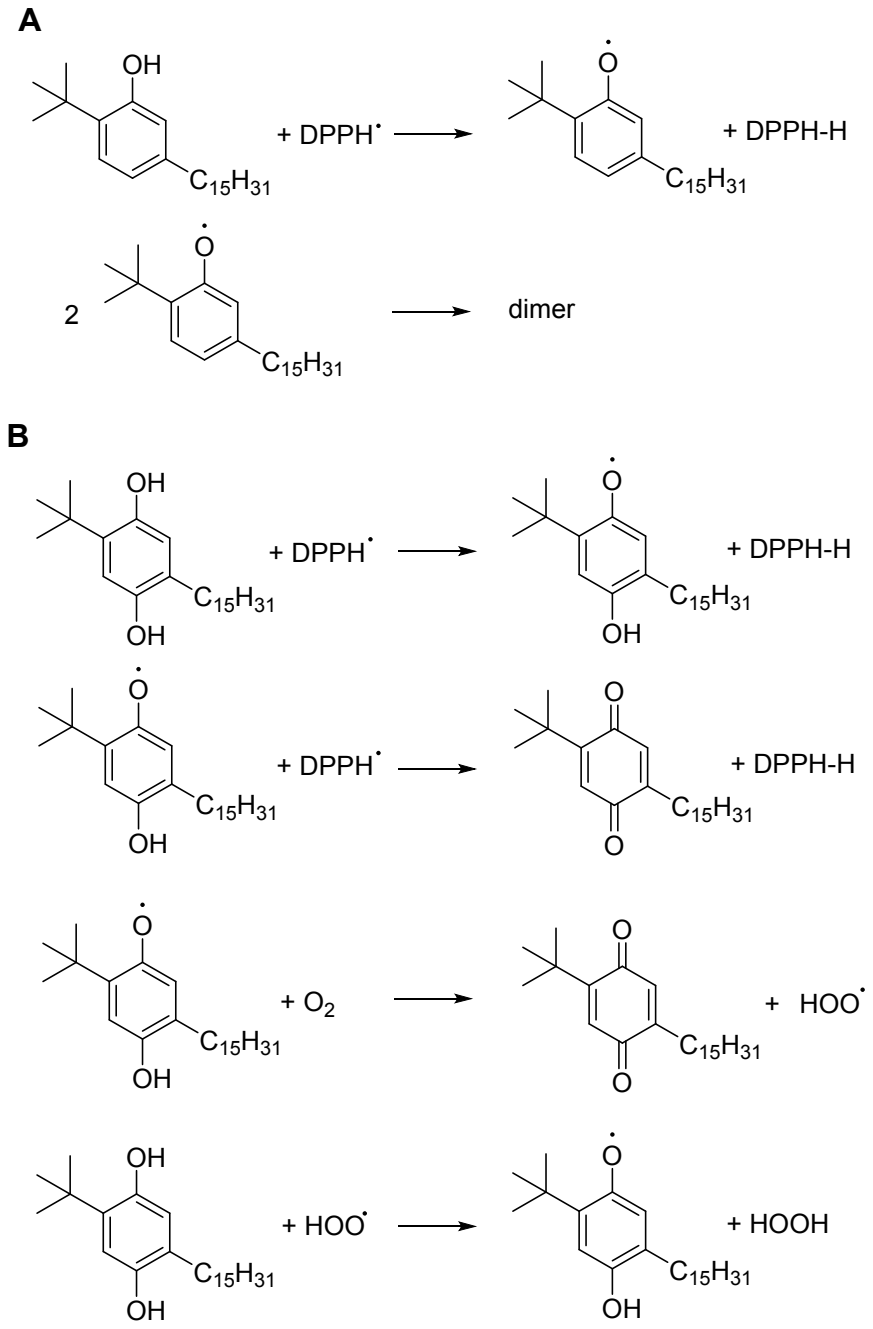

Figure 3. Mechanism for the reaction of DPPH with the monophenols (A) and hydroquinones (B) investigated in the present study.

Results, reported in Table 2, show that hydroquinone derivatives TB(OH)C and DTBQ are more reactive toward DPPH• than the monophenols TBC and BHT. As this difference is observed also

in the ~~homogeneous~~ chlorobenzene solution for the reaction with ROO•, it is due to the lower dissociation enthalpy of the O-H bonds of hydroquinones [~~56~~58]. Unexpectedly, in Triton X-100 micelles, TBC is about 50 times less reactive than BHT, whereas in ~~homogeneous~~ solution of chlorobenzene they have a similar antioxidant activity. This result can be explained by considering that the reaction between phenols and DPPH• is strongly accelerated in protic solvents by the onset of a sequential proton-loss electron transfer mechanism (SPLET) [~~57~~59]. The localization of DPPH• in the micelles can be determined by considering the position of its band centered at λ about 520 nm [~~34~~36]. It was reported that the absorbance of DPPH• shifts at higher wavelengths when increasing the water content of the medium due to an aggregation process [~~58~~60]. As shown in Fig S16 (SI), the normalized absorbance of DPPH• in the presence of micelles of Triton X-100 (1.0×10^{-3} M) is between the aggregate form ([Triton X-100] = 1.0×10^{-5} M, concentration of surfactant below CMC), and that of well solubilized molecules observed in organic solvents. This slightly shifted position and the broad shape of the DPPH band in the micellar system excludes that DPPH• is solubilized in the apolar interior of Triton X-100 micelles, and suggests that the radical is localized in the polyoxyethylene region, where DPPH• is exposed to water molecules, similarly to the localization of analogous 2,4,6-trinitrotoluene in Triton X-100 micelles [~~59~~61]. We suggest that the reaction of BHT with DPPH• is accelerated by the SPLET mechanism, while that of TBC is not. Actually, we found that moving from MeCN (polar aprotic) to MeOH containing 20% H_2O, the k_{DPPH} of BHT increases 20 times [~~60~~62], while that of TBC remains nearly constant (see Electronic Supplementary Information, Table S1). Moreover, the lower viscosity of BHT/Triton X-100 micelles with respect to TBC/Triton X-100 micelles may affect their relevant reactivity with DPPH• conferring a higher mobility to BHT in the shell layer with respect to TBC, that is, vice versa, anchored to the micellar core.

Table 2. Rate constants and stoichiometry of the reaction with DPPH• radicals in Triton X-100 13 mM micelles, and rate constant for the reaction with alkylperoxyl radicals in ~~homogeneous~~ organic solution.

Antioxidant	k_{dpph} ($M^{-1}s^{-1}$)	Stoichiometry	$k_{ROO\bullet}$ ($M^{-1}s^{-1}$)
TBC	8.5±3.0	1.0±0.1	3.2×10^{4} [a]
BHT	$(4.7\pm0.9)\times10^{2}$	1.3±0.2	2.6×10^{4} [a]
TB(OH)C	$(3.4\pm0.6)\times10^{3}$	0.5±0.1	3.6×10^{5} [a]
DTBQ	$(7\pm2)\times10^{3}$	0.8±0.1	1.6×10^{6} [b]

[a]50 °C, from reference 19; [b]30 °C, solvent chlorobenzene, from reference ~~55~~57.

The low stoichiometry of the reaction with DPPH• observed for TB(OH)C and DTBQ (Table 2) can be explained as due to the reaction of the semiquinone radical with oxygen (see Figure 3) [~~55~~57].

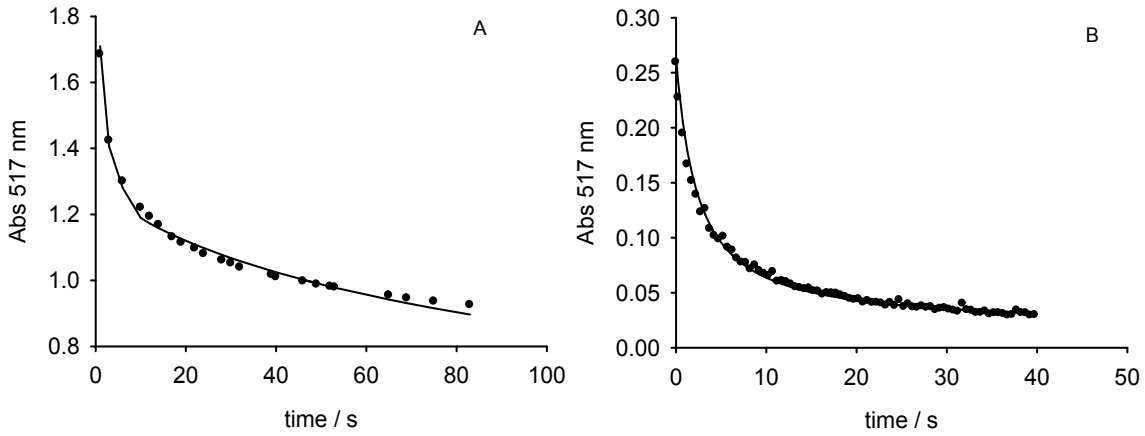

Figure 4. Decrease of the absorbance of DPPH• after the addition of (A) TBC or (B) TB(OH)C in cardanol/Triton X-100 micelles. Concentrations of cardanols are 1.0×10^{-4} M, those of DPPH• are

333 1.7×10^{-4} M and 2.4×10^{-5} M in graph A and B, respectively. Lines represent numerical fitting
334 obtained by the Gepasi software.
335
336 The antioxidant activity of the cardanol derivatives and that of the reference antioxidants was
337 assessed by verifying their ability to counteract the autoxidation of Triton X-100. Polyethylene
338 glycols are easily oxidized to hydroperoxides under air by a radical-chain reaction following the
339 same mechanism as that of peroxidation of lipids (see Figure 5) [~~61~~63, ~~62~~64].

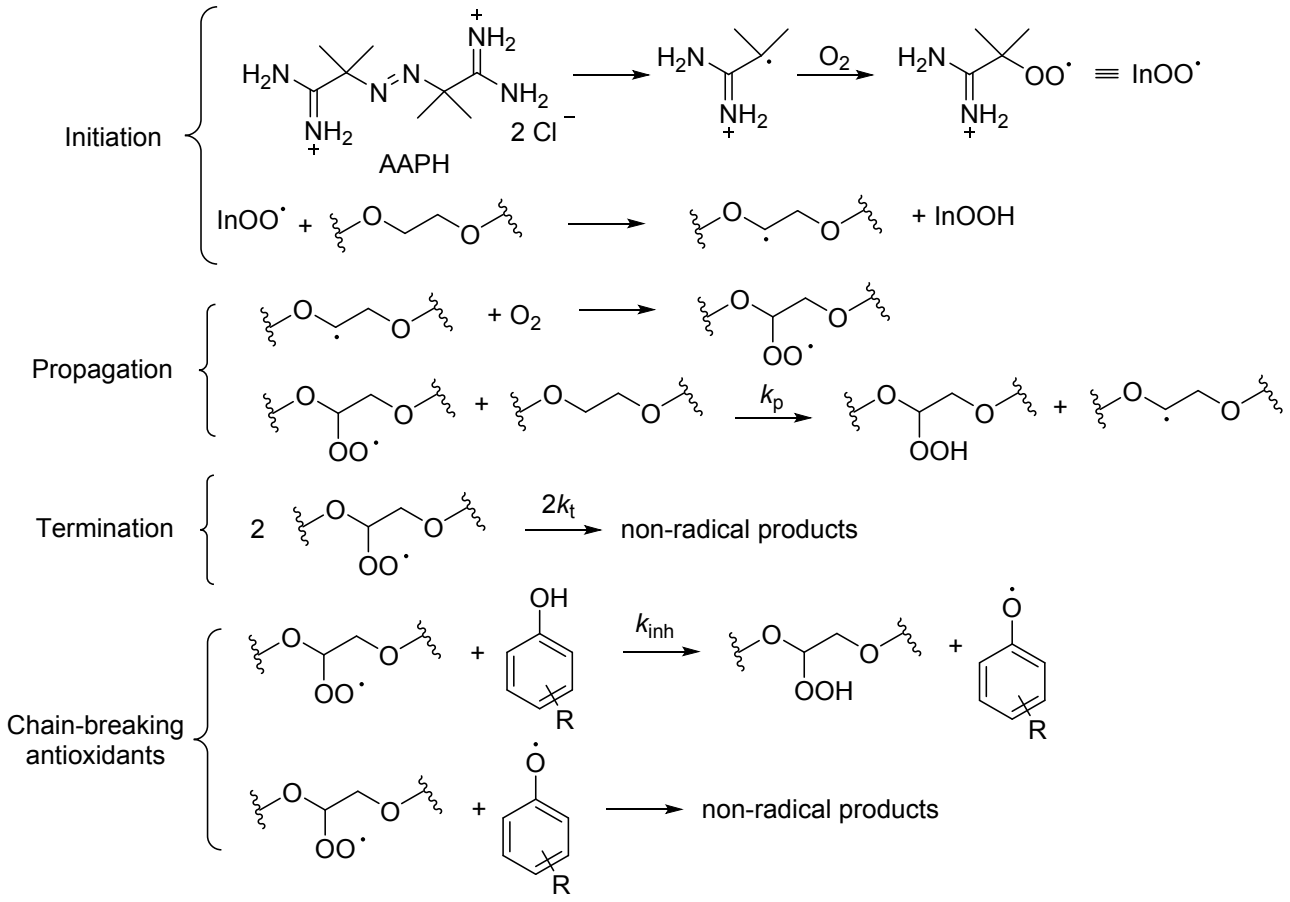
Initiation
AAPH
2 Cl
InOO
+ InOOH
Propagation
Termination
2
non-radical products
Chain-breaking antioxidants
non-radical products

340

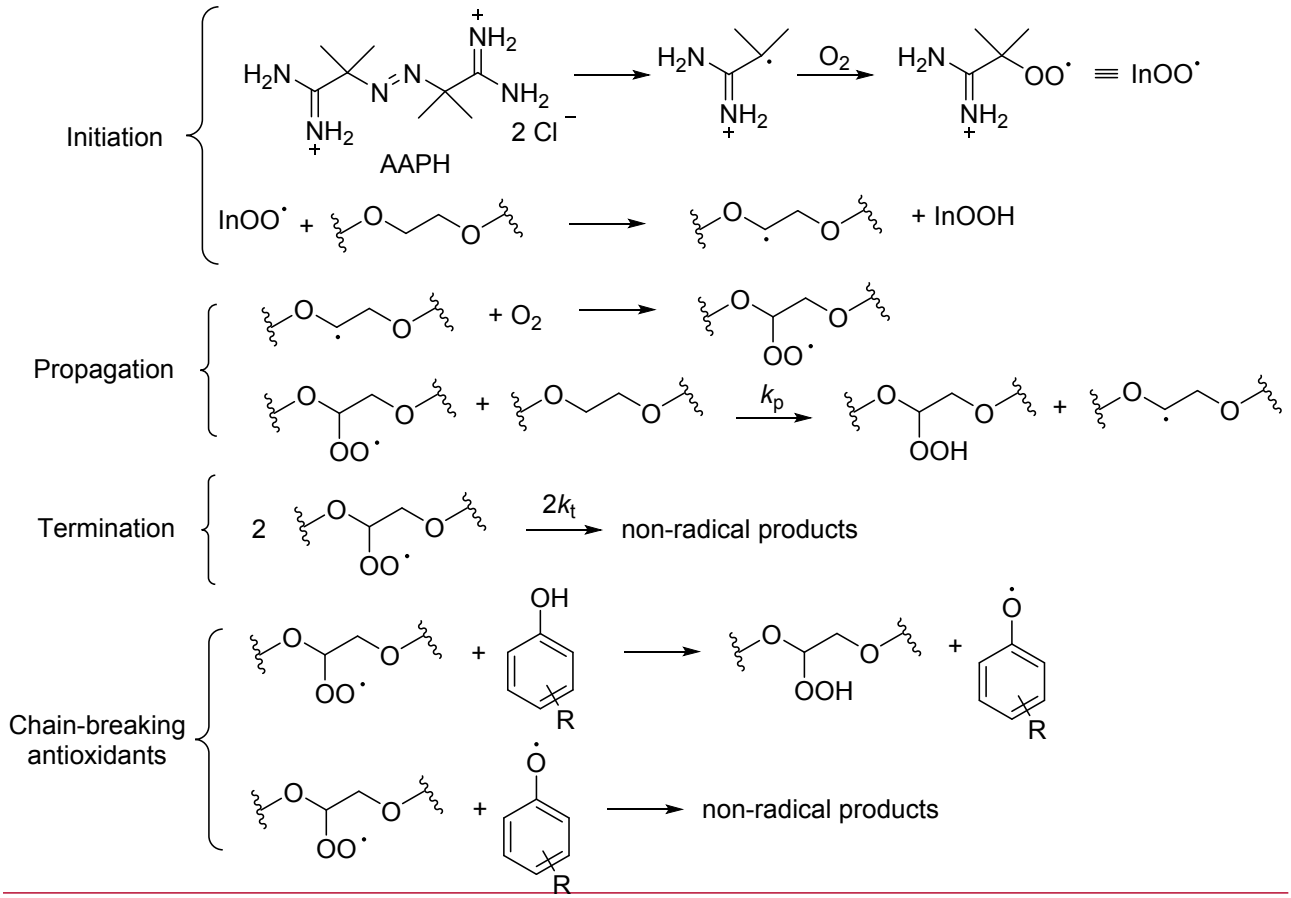

Figure 5. Autoxidation of the polyethylene glycol portion of Triton X-100 initiated by the thermal decomposition of AAPH and action of phenolic antioxidants.

The Triton X-100 autoxidation was initiated by the hydrosoluble azo-initiator 2,2′-Azobis(2-methylpropionamidine) dihydrochloride (AAPH) at 37 °C, and the formation of hydroperoxides was confirmed by using the ferrous xylenol orange assay on samples containing either AAPH or AAPH + Triton X-100 (see Figure 5 and Electronic Supplementary Information, Figure ~~S22~~S26). The reaction progress was followed by measuring the oxygen consumption by an automatic oxygen-uptake apparatus based on a differential pressure transducer [~~37~~39]. Typical plots of O_2 consumption are reported in Figure 6. In the absence of antioxidants, autoxidation of Triton X-100 causes a relatively fast linear oxygen consumption (R_0). The rate of radical generation (initiation

rate, R_i) was measured by the inhibitor method, and a R_i value of 3.7×10^{-9} M s^{-1} was obtained. The oxidizability of Triton X-100, i.e. the $k_p/(2k_t)^{1/2}$ value, could then be measured from equation 1, which describes the oxygen consumption R_0 of any given substrate (RH) as a function of its concentration and the value of R_i. The rate of oxidation in the presence of an antioxidant (AH) is instead described by equation 2,[19] where R_{inh} is the slope of oxygen consumption in the presence of the antioxidant, k_t is the rate constant for peroxyl radical termination, and k_{inh} is the rate constant for the reaction of the antioxidant with peroxyl radicals (see Figure 5).

$$R_0 = \frac{k_p}{\sqrt{2k_t}}[RH]\sqrt{R_i} \qquad \text{eq. 1}$$

$$\frac{R_0}{R_{inh}} = \frac{R_{inh}}{R_0} = \frac{2k_{inh}[AH]}{\sqrt{2k_tR_i}} \qquad \text{eq. 2}$$

~~$$-\frac{d[O_2]}{dt} = \frac{k_p}{\sqrt{2k_t}}[RH]\sqrt{R_i} \qquad \text{eq. 1}$$~~

The measured oxidizability of Triton X-100 (0.047 $M^{-1/2}$ $s^{-1/2}$) is comparable to that of other easily oxidizable compounds such as methyl linoleate (0.021 $M^{-1/2}$ $s^{-1/2}$) [~~37~~39], in agreement with previous reports of the ease of oxidation of polyethylene glycols. In fact, Triton X-100 possesses 9-10 repeated CH_2O units, accounting for 36-40 reactive H atoms. In the reasonable assumption that the $2k_t$ of Triton X-100 is the same observed for secondary peroxyl radicals (i.e. 10^6 M^{-1} s^{-1}) [~~37~~39], the k_p value of Triton X-100 can be estimated as 47 M^{-1} s^{-1}, that is 1.2 M^{-1} s^{-1} for each H atom, in good agreement with the k_p of ethers [~~63~~65].

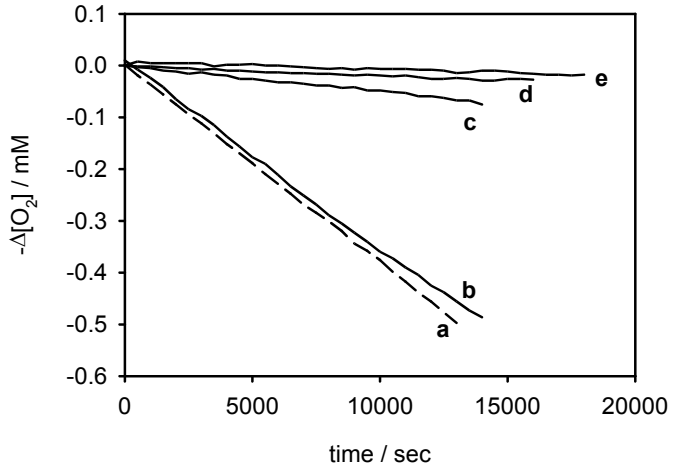

Figure 6. Oxygen consumption measured during the autoxidation of 13.2 mM Triton X-100 micelles (a) and Triton X-100 co-micellized with 10% of: DTBQ (b), TB(OH)C (c), TBC (d), BHT (e), initiated by AAPH (5 mM) at 37 °C in water.

In the presence of the co-micellized antioxidants, the oxygen consumption was strongly inhibited, except for DTBQ. The most active compounds were TBC and BHT, while TB(OH)C showed a smaller inhibition (see Figure 6). This result shows that mono-phenolic antioxidants, such as BHT and TBC, interrupt the radical chain of autoxidation by the two last reactions shown in Figure 5. The effect is very evident because of the large amount of phenol present in the system.

Surprisingly, hydroquinones which have a larger reactivity toward ROO• and DPPH• radicals than monophenolic derivatives, show a smaller antioxidant activity or no effect at all. The poor antioxidant properties of hydroquinones cannot be imputed to their difficulty to reach the palisade layer where reactive OCH_2 groups reside, as TBC/micelles are characterized by a similar high microviscosity. This result can be instead explained by superoxide ($O_2^{\bullet -}$/HOO•) formation (see Figure 3), in analogy with the experiments of DPPH• decay. Superoxide can propagate the oxidative chain, and cause the depletion of the antioxidant, or decay to H_2O_2 and O_2, depending

on the reaction conditions and on the localization of the antioxidant [~~55~~57, ~~64~~66]. The commercial antioxidant DTBQ although being the most active in ~~homogeneous~~ organic solution and in the DPPH• test, has the weakest activity in micelles, whereas TBC has an activity superimposable to that of BHT. Interestingly, if comparing the commercial DTBD and the cardanol-derived hydroquinones TB(OH)C, the latter has a stronger activity than the former, presumably as effect of small differences in the localization of the respective semiquinone radicals. It may be suggested that the formation of superoxide by semiquinones is facilitated by water, because it promotes the deprotonation of the semiquinone (pKa≈4) [~~55~~57].

By using the kinetic equation describing the oxygen consumption during the autoxidation of an organic substrate in the presence of an antioxidant (equation 2) [19], it was possible to obtain the rate constants for the reaction of TBC with peroxyl radicals in our system (k_{inh}) as 480 $M^{-1}s^{-1}$. The knowledge of k_{inh} allowed us to predict the inhibition degree at different TBC concentrations by using equation 2. For instance, 5 % and 10% TBC are able to slow down the Triton-X100 autoxidation by about 10 and 20 times, respectively. A proportionally weaker inhibition can be achieved if employing a smaller antioxidant concentration. Of course, the amount of cardanols to be added to Triton X-100 will depend on the antioxidant protection required for each specific application.

4. Conclusions

In the present study we demonstrated through tensiometric measurements, DLS analysis, polarity and microviscosity determinations that hydrogenated cardanol derived guests do reside in the polar corona region of Triton X-100 micelles. Thanks to this arrangement they can act as good antioxidants reacting with DPPH• in the same micellar polar region and reducing the autoxidation of polyoxyethylene chains of macromolecular surfactant Triton X-100. Compared to previous

studies carried out in ~~homogeneous~~ organic solvents, the novelty of the present research work is that the antioxidant activity of the investigated cardanol derivatives is assessed in a micellar environment. In these conditions, the antioxidant activity is in fact strongly influenced by the localization of the radical-trapping agent in the aggregate.

Since pegylated derivatives are widely used in cosmetic products as surfactants, emulsifiers, cleansing agents, humectants, and skin conditioners [~~65~~67] as well as in drug delivery carriers because pegylated nanoparticles demonstrated to avoid the reticuloendothelial system activation and allow to increase the circulatory time and reducing renal clearance of nanoparticles,[~~66~~68-~~68~~70] the here demonstrated ability of green and renewable cardanol derivatives to protect them from oxidation is an important outcome.

Conflict of interest

There are no conflicts to declare.

Electronic Supplementary Information

Electronic Supplementary Information: ^{1}H and ^{13}C NMR spectra of TBC and TB(OH)C, ~~Tensiometric~~ tensiometric data, spectrofluorimetric determination of aggregation number and viscosity, spectrophotometric spectra and Dynamic Light Scattering (DLS), determination of DPPH• scavenging, solvent effect on the reaction between DPPH• and monophenolic antioxidants, Triton X-100 autoxidation evidences. This material is available free.

Acknowledgement

We thank Università “G. d’Annunzio” of Chieti-Pescara and Università degli studi of Bologna for funding, and Prof. O. Attanasi for providing cardanol samples.

Abbreviations: PEG, polyethylene-glycol; BHA, butylated hydroxyanisole; BHT butylated hydroxyl-toluene; PG, propyl gallate; TBHQ, *tert*-butyl-hydroquinone; DTBQ, 2,5-di-*tert*-butylhydroquinone; NPEs, nonyl phenol ethoxylates; LABs, alkyl benzenes; TBC, 6-*tert*-butyl hydrogenated cardanol; TB(OH)C, 6-*tert*-butyl-4-hydroxy hydrogenated cardanol; CMC, critical micelle concentration; DPPH•, 2,2-diphenyl-1-picrylhydrazyl radical; PMHC, 2,2,5,7,8-pentamethyl-6-chromanol; AAPH, 2,2′-Azobis(2-methylpropionamidine) dihydrochloride; CNSL, Cashew Nut Shell Liquid.

REFERENCES

[1] Tan, J. S.; Butterfield, D. E.; Voycheck, C. L.; Caldwell, K. D.; Li, J. T. Surface modification of nanoparticles by PEO/PPO block copolymers to minimize interactions with blood components and prolong blood circulation in rats, *Biomaterials*, **1993**, *14*, 823–833.

[2] Klibanov, A. L.; Maruyama, K.; Torchilin, V. P.; Huang, L. Amphipathic polyethyleneglycols effectively prolong the circulation time of liposomes. *FEBS Lett*., **1990**, *268*, 235–237.

[3] Suk, J. S.; Xu, Q.; Kim, N.; Hanes, J.; Ensign. L. M. PEGylation as a strategy for improving nanoparticle-based drug and gene delivery, *Adv. Drug Deliv. Rev*., **2016**, *99*, 28–51.

[4] Meunier, M.; Goupil, A.; Lienard, P. Predicting drug loading in PLA-PEG nanoparticles. *Int. J. Pharm.* **2017**, *526*, 157–166.

[5] Duncan, T. V. Applications of nanotechnology in food packaging and food safety: Barrier materials, antimicrobials and sensors. *J. Colloid Interface Sci*., **2011**, *363*, 1–24.

[6] Apicella, A.; Cappello, B.; Del Nobile, M. A.; La Rotonda, M. I.; Mensitieri, G.; Nicholais, L. Poly(Ethylene oxide) (PEO) and different molecular weight PEO blends monolithic devices for drug release. *Biomaterials*, **1993**, *14*, 83–90.

[7] Han, S.; Kim, C.; Kwon, D. Thermal/oxidative degradation and stabilization of polyethylene glycol. *Polymer* **1997**, *38(2)*, 317–323.

[8] Vrandečić, N. S.; Erceg, M.; Jakić, M.; Klarić, I. Kinetic analysis of thermal degradation of poly(ethylene glycol) and poly(ethylene oxide)s of different molecular weight. *Thermochim. Acta*, **2010**, *498*, *71–80*.

[9] Kazunori, E.; Van Alstine, J. M.; Harris, J. M. Stability of Poly(ethylene glycol) Graft Coatings. *Langmuir*, **1998**, *14(10)*, 2722-2729.

[10] Stein, D.; Bindra, D. S. Stabilization of Hard Gelatin Capsule Shells Filled with Polyethylene Glycol Matrices. *Pharm. Dev. Technol.*, **2007**, *12(1)*, 71-77.

[11] Makahleh, A; Saad, B.; Bari, M.F. Synthetic phenolics as antioxidants for food preservation in *Handbook of Antioxidants for Food Preservation*, ed. S. Fereidoon, Woodhead Publishing Series in Food Science, Technology and Nutrition, Cambridge, UK, 1st edition, 2015, ch. 3, 51–78.

[12] Fereidoon, S.; Ambigaipalan, P. Phenolics and polyphenolics in foods, beverages and spices: Antioxidant activity and health effects – A review. *J. Funct. Foods* **2015**, *18*, 820–897.

[13] Leclercq, C.; Arcella, D.; Turrini, A. Estimates of the theoretical maximum daily intake of erythorbic acid, gallates, butylated hydroxyanisole (BHA) and butylated hydroxytoluene (BHT) in Italy: a stepwise approach. *Food Chem. Toxicol.* **2000**, *38(12)*, 1075–1084.

[14] Thanitwatthanasak, S; Sagis, L. M. C.; Chitprasert, P. Pluronic F127/Pluronic P123/vitamin E TPGS mixed micelles for oral delivery of mangiferin and quercetin: Mixture-design optimization, micellization, and solubilization behavior. *J. Mol. Liq*. **2019**, *274*, 223–238.

[15] Xu, D-P.; Li, Y.; Meng, X.; Zhou, T.; Zhou, Y.; Zheng, J.; Zhang, J.-J.; Li, H.-B. Natural Antioxidants in Foods and Medicinal Plants: Extraction, Assessment and Resources. *Int. J. Mol. Sci.* **2017**, *18,* Article 96, 1–32.

[16] G. Vasapollo, G. Mele, R. Del Sole, Cardanol-Based Materials as Natural Precursors for Olefin Metathesis. *Molecules* **2011**, *16(8)*, 6871−6882.

[17] Balachandran, V. S.; Jadhav, S. R.; Vemula, P. K.; John, G. Recent advances in cardanol chemistry in a nutshell: From a nut to nanomaterials. *Chem. Soc. Rev.* **2013**, *42-(2)*, 427–438.

[18] Liu, R.; Zhu, G.; Li, Z.; Liu, X.; Chen, Z.; Ariyasivam, S. Cardanol-based oligomers with "hard core, flexible shell" structures: from synthesis to UV curing applications. *Green Chem*., **2015**, *17*, 3319–3325.

[19] Attanasi, O. A.; Filippone, P.; Fiorucci, C.; Saladino, R.; Amorati, R.; Pedulli, G. F.; Valgimigli, L. Absolute rate constants for the reaction of peroxyl radicals with cardanol derivatives. *J. Chem. Soc.,Perkin Trans. 2* **2001**, 2142–2146.

[20] Amorati, R.; Attanasi, O. A.; El Ali, B.; Filippone, P.; Mele, G.; Spadavecchia, J.; Vasapollo, G. Synthesis of New Cardanol and Cardol Derivatives by Allylation and Regioselective Cyclocarbonylation Reactions. *Synthesis* **2002**, *18*, 2749–2755.

[21] Amorati, R.; Attanasi, O. A.; Favi, G.; Menichetti, S.; Pedulli, G. F.; Viglianisi, C.; Amphiphilic antioxidants from "cashew nut shell liquid" (CNSL) waste. *Org. Biomol. Chem.* **2011**, *9*, 1352–1355.

[22] Liu, Z.; Chen, J.; Knothe, G.; Nie, X.; Jiang, J. Synthesis of Epoxidized Cardanol and Its Antioxidative Properties for Vegetable Oils and Biodiesel, *ACS Sustainable Chem. Eng*. **2016**, *4(3)*, 901–906.

[23] Feng, J.; Zhao, H.; Yue, S.; Liu, S. One-Pot Synthesis of Cardanol-Derived High-Efficiency Antioxidants Based on Intramolecular Synergism, *ACS Sustainable Chem. Eng.* **2017**, *5*, 3399−3408.

[24] Blunk, D.; Bierganns, P.; Bongartz, N.; Tessendorf, R.; Stubenrauch, C. New speciality surfactants with natural structural motifs. *New J. Chem.* **2006**, *30*, 1705–1717.

[25] Deshpande, N. U.; Jayakannan, M. Biotin-tagged polysaccharide vesicular nanocarriers for receptor mediated anticancer drug delivery in cancer cells. *Biomacromolecules* **2018**, *19*, 3572–3585.

[26] Montenegro, C. E.; Carioca, J. O. B.; Attanasi, O. A.; Filippone, P.; Correra, R. G. C.; Correra, F. R.; Araujo de Abreu, R. F. Production process of alkylated antioxidant, obtained from phenols and cresols, preferably of hydrogenated cardanol, 3-pentadecylphenol (3-PDP) applicable as additive in fuels and lubricants**.** Patent no. BR2002011378, **2017**.

[~~25~~27] Soares, A.; Guieysse, B.; Jefferson, B.; Cartmell, E.; Lester, J. N. Nonylphenol in the environment: a critical review on occurrence, fate, toxicity and treatment in wastewaters. *Environ. Int*. **2008**, *34*, 1033–1049.

[~~26~~28] Fontana, A.; Guernelli, S.; Zaccheroni, N.; Zappacosta, R.; Genovese, D.; De Crescentini, L.; Riela, S. Micellization properties of cardanol as a renewable co-surfactant. *Org. Biomol. Chem.* **2015**, *13*, 9214–9222.

[~~27~~29] Massaro, M.; Riela, S.; Guernelli, S.; Parisi, F.; Lazzara, G.; Baschieri, A.; Valgimigli, L.; Amorati, R. A synergic nanoantioxidant based on covalently modified halloysite–trolox nanotubes with intra-lumen loaded quercetin. *J. Mater. Chem. B~~,~~* **2016**, *4*, 2229–2241.

[~~28~~30] Massaro, M.; Amorati, R.; Cavallaro, G.; Guernelli, S.; Lazzara, G.; Milioto, S.; Noto, R.; Poma, P.; Riela, S. Direct chemical grafted curcumin on halloysite nanotubes as dual responsive prodrug for pharmacological applications. *Colloids Surf.~~,~~ B* **2016**, *140*, 505–513.

[~~29~~31] Attanasi, O. A.; Filippone, P.; Balducci, S. Effect of metal ions in organic synthesis. XXXV: Simple and convenient aromatic alkylation of some alkenylphenol derivatives with *tert*alkyl methyl ethers in the presence of Tin(IV)chloride. *Gazz. Chim. Ital*. **1991**, *121*, 487–489.

[~~30~~32] Saladino, R.; Neri, V.; Mincione, E.; Marini, S.; Coletta, M.; Fiorucci, C.; Filippone, P. A new and efficient synthesis of ortho- and para-benzoquinones of cardanol derivatives by the catalytic system $MeReO_3$-H_2O_2. *J. Chem. Soc., Perkin Trans. 1* **2000**, 581–586.

[~~31~~33] Turro, N. J; Yekta, A. Luminescent probes for detergent solutions. A simple procedure for
determination of the mean aggregation number of micelles. *J. Am. Chem. Soc*. **1978**, *100*, 5951–5952.

[~~32~~34] Winnik, F. M.; Regismond, S. T. A. Fluorescence methods in the study of the interactions of surfactants with polymers. *Colloids Surf. A – Physicochem. Eng. Asp*. **1996**, *118(1–2)*,1–39.

[~~33~~35] Cerritelli, S.; Fontana, A.; Velluto, D.; Adrian, M.; Dubochet, J.; De Maria, P.; Hubbell, J. A. Thermodynamic and Kinetic Effects in the Aggregation Behavior of a Poly(ethylene glycol-*b*-propylene sulfide-β−ethylene glycol) ABA Triblock Copolymer. *Macromolecules~~,~~* **2005**, *38*, 7845–7851.

[~~34~~36] Amorati, R.; Valgimigli, L. Advantages and limitations of common testing methods for antioxidants. *Free Radic. Res*. **2015**, *49(5)*, 633–649.

[~~35~~37] Mendes, P .Biochemistry by numbers: simulation of biochemical pathways with Gepasi 3, *Trends Biochem. Sci.* **1997**, *22*, 361–363.

[~~36~~38] Foti, M. C.; Daquino, C. Kinetic and thermodynamic parameters for the equilibrium reactions of phenols with the DPPH• radical. *Chem. Commun.* **2006**, 3252–3254.

[~~37~~39] Amorati, R.; Baschieri, A.; Valgimigli. L., Measuring Antioxidant Activity in Bioorganic Samples by the Differential Oxygen Uptake Apparatus: Recent Advances. *J. Chemistry* **2017**, Article ID 6369358, 1–12.

[~~38~~40] Baschieri, A.; Pulvirenti, L.; Muccilli, V.; Amorati, R.; Tringali, C. Chain-breaking antioxidant activity of hydroxylated and methoxylated magnolol derivatives: the role of H-bonds. *Org. Biomol. Chem.* **2017**, *15*, 6177–6184.

[~~39~~41] Clint, J. H. *Surfactant Aggregation*, Blackie & Son Ltd: London, **1992**, p. 119.

[~~40~~42] Yazu, K.; Yamamoto, Y.; Niki, E.; Mikia, K.; Ukegaw, K. Mechanism of lower oxidizability of eicosapentaenoate than linoleate in aqueous micelles. II. Effect of antioxidants. *Lipids~~,~~* **1998**, *33(6)*, 597-600.

[41~~43~~] Alauddin, M.; Verrall, R, E. Apparent molal volume and solubility studies of 2,6-di-*tert*-butyl-4-methylphenol, 2-*tert*-butyl-4-methoxyphenol, and 2,6-di-*tert*-butyl-4-(hydroxymethyl) phenol in aqueous micelle solutions of poly(oxyethylene) (23) lauryl ether as a function of micelle concentration and temperature, *J. Phys. Chem*. **1987**, *91(7)*, 1802-1809.

[42~~44~~] Torres, V. M.; Posa, M.; Srdjenovic, B.; Simplício, A. L. Solubilization of fullerene C_{60} in micellar solutions of different solubilizers, *Colloid Surf. B-Biointerfaces*, 2011, **82**(1), 46-53.

[43~~45~~] Dharaiya, N.; Bahadur, P. Phenol induced growth in Triton X-100 micelles: effect of pH and phenols hydrophobicity. *Colloid Surf. A-Physicochem. Eng. Asp.* **2012**, *410*, 81–90.

[44~~46~~] Patel, U.; Dharaiya, N.; Bahadur, P. Preservative solubilization induces microstructural change of Triton X-100 micelles. *J. Mol. Liq*. **2016**, *216*, 156–163

[45~~47~~] Turro, N. J.; Kuo, P. L. Fluorescence Probes for Aqueous Solutions of Nonionic Micelles, *Langmuir* **1985**, *1*, 170–172.

[46~~48~~] Bernardez, L. A.; Ghoshal, S. Selective Solubilization of Polycyclic Aromatic Hydrocarbons from Multicomponent Nonaqueous-Phase Liquids into Nonionic Surfactant Micelles. *Environ. Sci. Technol.* **2004**, *38*, 5878–5887.

[47~~49~~] Cong Dong, D.; Winnik, M. A. The Py scale of solvent polarities. *Can. J. Chem.* **1984**, *62*, 2560–2565.

[48~~50~~] Ruiz, C.C.; Aguiar, J. Interaction, stability and microenvironmental properties of mixed micelles of Triton X-100 and n-alkyltrimethylammonium bromides: influence of alkyl chain length, *Langmuir* **2000**, *16*, 7946–7953.

[~~49~~51] Han, S. K.; Kim, J.-S.; Lee, Y.-S.; Kim, M. Effect of Drug Substances on the Microviscosity of Lipid Bi|ayer of Liposomal Membrane, *Arch. Pharm. Res.* **1990**, *13(2)*, 192–197.

[~~50~~52] Behera, K.; Pandey, M. D.; Porel, M.; Pandey, S. Unique role of hydrophilic ionic liquid in modifying properties of aqueous Triton X-100, *J. Chem. Phys*. **2007**, *127*, Article 184501, 1–10.

[~~51~~53] Garcio-Blanco, F.; Elorza, M.A.; Arias, C., Elorza, B.; Gomez-Escalonilla, I.; Civera, C.; Galera-Gomez, P. A. Interaction of 2,2,2-trifluoroethanol with aqueous micelles of Triton X-100, *J. Coll. Interface Sci.* **2009**, *330*, 163–193.

[~~52~~54] Gharibi, H.; Sohrabi, B.; Javadian, S.; Hashemianzadeh, M. Study of the electrostatic and steric contributions to the free energy of ionic/nonionic mixed micellization, *Colloid Surf. A – Physicochem. Eng. Asp*. **2004,** *244*, 187–196.

[~~53~~55] Vuorte, M.; Maatta, J.; Sammalkorpi, M. Simulations Study of single-component and mixed n⊠alkyl-PEG Micelles, *J. Phys. Chem. B* **2018**, *122*, 4851−4860.

[~~54~~56] Foti, M. C. Use and Abuse of the DPPH• Radical. *J. Agric. Food Chem.* **2015**, *63*, 8765−8776.

[~~55~~57] L Valgimigli, L.; Amorati, R.; Fumo, M. G.; DiLabio, G. A.; Pedulli, G. F.; Ingold, K. U.; Pratt, A. D. The Unusual Reaction of Semiquinone Radicals with Molecular Oxygen. *J. Org. Chem.* **2008**, *73*, 1830–1841.

[~~56~~58] Lucarini, M.; Pedulli, G. F. Free radical intermediates in the inhibition of the autoxidation reaction. *Chem. Soc. Rev.* **2010**, *39*, 2106–2119.

[~~57~~59] Liwinienko, G.; Ingold, K. U. Solvent Effects on the Rates and Mechanisms of Reaction of Phenols with Free Radicals. *Acc. Chem. Res.* **2007**, *40*, 222–230.

[~~58~~60] Sanna, D.; Delogu, G.; Mulas, M.; Schirra, M.; Fadda, A. Determination of Free Radical Scavenging Activity of Plant Extracts Through DPPH Assay: An EPR and UV–Vis Study. *Food Anal. Methods.***2012,** *5*, 759–766.

[~~59~~61] Luning Prak, D. J.; Jahraus, W. I.; Sims, J. M.; Roy MacArthur, A. H. An ^{1}H NMR investigation into the loci of solubilization of 4-nitrotoluene, 2,6-dinitrotoluene, and 2,4,6-trinitrotoluene in nonionic surfactant micelles, *Colloid Surf. A-Physicochem. Eng. Asp.* **2011**, *375*, 12–22.

[~~60~~62] Musialik, M.; Litwinienko,G. Scavenging of DPPH• radicals by vitamin E is accelerated by its partial ionization: the role of sequential proton loss electron transfer. *Org. Lett.* **2005**, *7*, 4951-4954.

[~~61~~63] Mantzavinos, D.; Livingston, A. G.; Hellenbrand, R.; Metcalfe, I, S. Wet air oxidation of polyethylene glycols; mechanisms, intermediates and implications for integrated chemicalbiological wastewater treatment. *Chem. Eng. Sci.* **1996**, *51(18)*, 4219–4235.

[~~62~~64] Seongok, H.; Chongyoup K.; Dongsook K. Thermal/oxidative degradation and stabilization of polyethylene glycol. *Polymer* **1997**, *38*, 317–323.

[~~63~~65] Amorati, R.; Baschieri, A.; Morroni, G.; Gambino, R.; Valgimigli, L. Peroxyl Radical Reactions in Water Solution: A Gym for Proton-Coupled Electron-Transfer Theories. *Chem. Eur. J.* **2016**, *22*, 7924–7934.

[~~64~~66] Cedrowski, J.; Litwinienko, G.; Baschieri, A.; Amorati, R. Hydroperoxyl Radicals (HOOC): Vitamin E Regeneration and H-Bond Effects on the Hydrogen Atom Transfer. *Chem. Eur. J.* **2016**, *22*, 16441–16445.

[~~65~~67] Jang, H.-J.; Shin, C. Y.; Kim, K.-B. Safety Evaluation of Polyethylene Glycol (PEG) Compounds for Cosmetic Use. *Toxicol. Res.* **2015**, *31(2)*, 105–136.

[~~66~~68] Perez, A. T.; Domenech, G. H.; Frankel, C.; Vogel, C. L. Pegylated liposomal doxorubicin (Doxil) for metastatic breast cancer: the Cancer Research Network, Inc., experience. *Cancer Invest.* **2002**, *20*, 22–29.

[~~67~~69] Di Crescenzo, A.; Aschi, M.; Fontana, A. Toward a better understanding of steric stabilization when using block copolymers as stabilizers of single-walled carbon nanotubes (SWCNTs) aqueous dispersions, *Macromolecules* **2012**, *45*, 8043–8050.

[~~68~~70] Di Meo, E. M.; Di Crescenzo, A.; Velluto, D.; O'Neil, C. P.; Demurtas, D.; Hubbell, J. A.; Fontana, A. Assessing the role of poly(ethylene glycol-*bl*-propylene sulfide) (PEG-PPS) block copolymers in the preparation of carbon nanotube biocompatible dispersions, *Macromolecules* **2010**, *43*, 3429–3437.

Supplementary Material Description:

~~**SUPPORTING INFORMATION**~~

S1. ^{1}H and ^{13}C NMR spectra (page S3-S7): Fig. S1. ^{1}H NMR spectrum of TBC, Fig S2. ^{13}C NMR spectrum of TBC, Fig. S3. ^{1}H NMR spectrum of TB(OH)C, Fig S4. ^{13}C NMR spectrum of TB(OH)C.

S2. CMC determinations (page ~~S3~~S8-~~S5~~S10): Fig ~~S1~~S5. TBC/Triton X-100, Fig ~~S2~~S6. TB(OH)C/Triton X-100, Fig ~~S3~~S7. BHT/Triton X-100, Fig ~~S4~~S8. DTBQ/Triton X-100

~~S2~~S3. Determination of aggregation Number (page ~~S6~~S11-~~S7~~S12): Fig ~~S5~~S9. TBC/Triton X-100, Fig ~~S6~~S10. TB(OH)C/Triton X-100, Fig ~~S7~~S11. BHT/Triton X-100, Fig ~~S8~~S12. DTBQ/Triton X-100

~~S3~~S4. Determination of microviscosity (page ~~S8~~S13-~~S10~~S15): Fig ~~S9~~S13. Pure Triton X-100, Fig ~~S10~~S14. Cardanol/Triton X-100, Fig ~~S11~~S15. TBC/Triton X-100, Fig ~~S12~~S16. TB(OH)C/Triton X-100, Fig ~~S13~~S17. BHT/Triton X-100, Fig ~~S14~~S18. DTBQ/Triton X-100

~~S4~~S5. Fluorescence spectra of pyrene in the presence of DPPH (page ~~S11~~S16): Fig ~~S15~~S19.

~~S5~~S6. Micelles Characterization: Dynamic Light Scattering (DLS) (page ~~S11~~S16-~~S13~~S18): Fig S20~~16~~. Triton X 100 10^{-3} M, Fig ~~S17~~S21. Triton X 100 10^{-3} M/TBC 10%, Fig ~~S18~~S22. Triton X 100 10^{-3} M/TB(OH)C 10%, Fig ~~S19~~S23. Triton X 100 10^{-3} M/BHT 10%, Fig ~~S20~~S24. Triton X 100 10^{-3} M/DTBQ 10%

~~S6~~S7. UV-Vis spectra of DPPH• radical in different media (page ~~S14~~S19): Fig ~~S21~~S25.

~~S7~~S8. Determination of DPPH scavenging (page ~~S14~~S19): Table S1. Solvent effect on the reaction between DPPH• and monophenolic antioxidants

~~S8~~S9. Kinetic analysis of DPPH• experiments (page ~~S15~~S20-~~S16~~S21)

~~S9~~S10. Triton X-100 autoxidation (page ~~S16~~S21): Fig ~~S22~~S26.

Cardanol-like co-surfactants solubilized in pegylated micelles keep their antioxidant activity and preserve polyethylene glycol chains from oxidation

Antonella Fontana,[a*] Susanna Guernelli,[b*] Antonello Di Crescenzo,[a] Pietro Di Profio,[a] Francesco Palomba,[b] Lucia De Crescentini,[c] Riccardo Amorati [b] and Andrea Baschieri [b]

[a]*Dipartimento di Farmacia, Università "G. d'Annunzio", Via dei Vestini 31, 66100 Chieti, Italy*

[b]*Dipartimento di Chimica "G. Ciamician", Università degli Studi di Bologna, Via S. Giacomo 11 and Via Selmi 2, 40126 Bologna, Italy*

[c]*Dipartimento di Scienze Biomolecolari, Università di Urbino "Carlo Bo", Via Maggetti 24, 60129 Urbino, Italy*

Electronic Supplementary Material

S1. ^{1}H and ^{13}C NMR spectra of cardanol derivatives

General Information. Analytical grade solvents and commercially available reagents were used as received unless otherwise stated. ^{1}H and ^{13}C NMR spectra were recorded on Varian Mercury (400 MHz for ^{1}H) spectrometer. Chemical shifts (δ) are reported in ppm relative to residual solvent signals for ^{1}H and ^{13}C NMR (^{1}H NMR: 7.27 ppm and ^{13}C NMR: 77.0 ppm for $CDCl_3$). ^{13}C NMR spectra were acquired with ^{1}H broadband decoupled mode. Coupling constants are given in Hz.

TBC

^{1}H NMR ($CDCl_3$, 400 MHz) δ 7.17 (d, J = 7.9 Hz, 1H), 6.70 (dd, J = 8.0 Hz, J = 1.8 Hz, 1H), 6.50 (d, J = 1.8 Hz, 1H), 4.64 (bs, 1 OH), 2.51 (t, J = 7.7 Hz, 2H), 1.63 – 1.56 (m, 2H), 1.40 (s, 9H), 1.28 – 1.26 (m, 24H), 0.89 (t, J = 6.8 Hz, 3H).

^{13}C NMR ($CDCl_3$, 100 MHz) δ 153.9 (C), 142.1 (C), 133.2 (C), 126.9 (CH), 120.5 (CH), 116.6 (CH), 35.1 (CH_2), 34.2 (C), 32.0 (CH_2), 31.3 (CH_2), 29.7 (5 CH_2), 29.7_1 (CH_3), 29.6_8 (CH_2), 29.6_3 (CH_2), 29.5_6 (CH_2), 29.5 (CH_2), 29.4 (CH_2), 22.7 (CH_2), 14.1 (CH_3).

TB(OH)C

^{1}H NMR ($CDCl_3$, 400 MHz) δ 6.70 (s, 1H), 6.45 (s, 1H), 4.36 (bs, 1 OH), 4.24 (bs, 1 OH), 2.50 (t, J = 7.8 Hz, 2H), 1.63 – 1.55 (m, 2H), 1.38 (s, 9H), 1.30 – 1.26 (m, 24H), 0.89 (t, J = 6.8 Hz, 3H).

^{13}C NMR ($CDCl_3$, 100 MHz) δ 147.8 (C), 146.7 (C), 134.7 (C), 126.6 (C), 117.9 (CH), 114.4 (CH), 34.2 (C), 31.9 (CH_2), 29.8 (CH_2), 29.6_9 (5 CH_2), 29.6_6 (2 CH_2), 29.6 (CH_2), 29.5_9 (CH_3), 29.5_5 (CH_2), 29.4 (CH_2), 29.3 (CH_2), 22.7 (CH_2), 14.1 (CH_3).

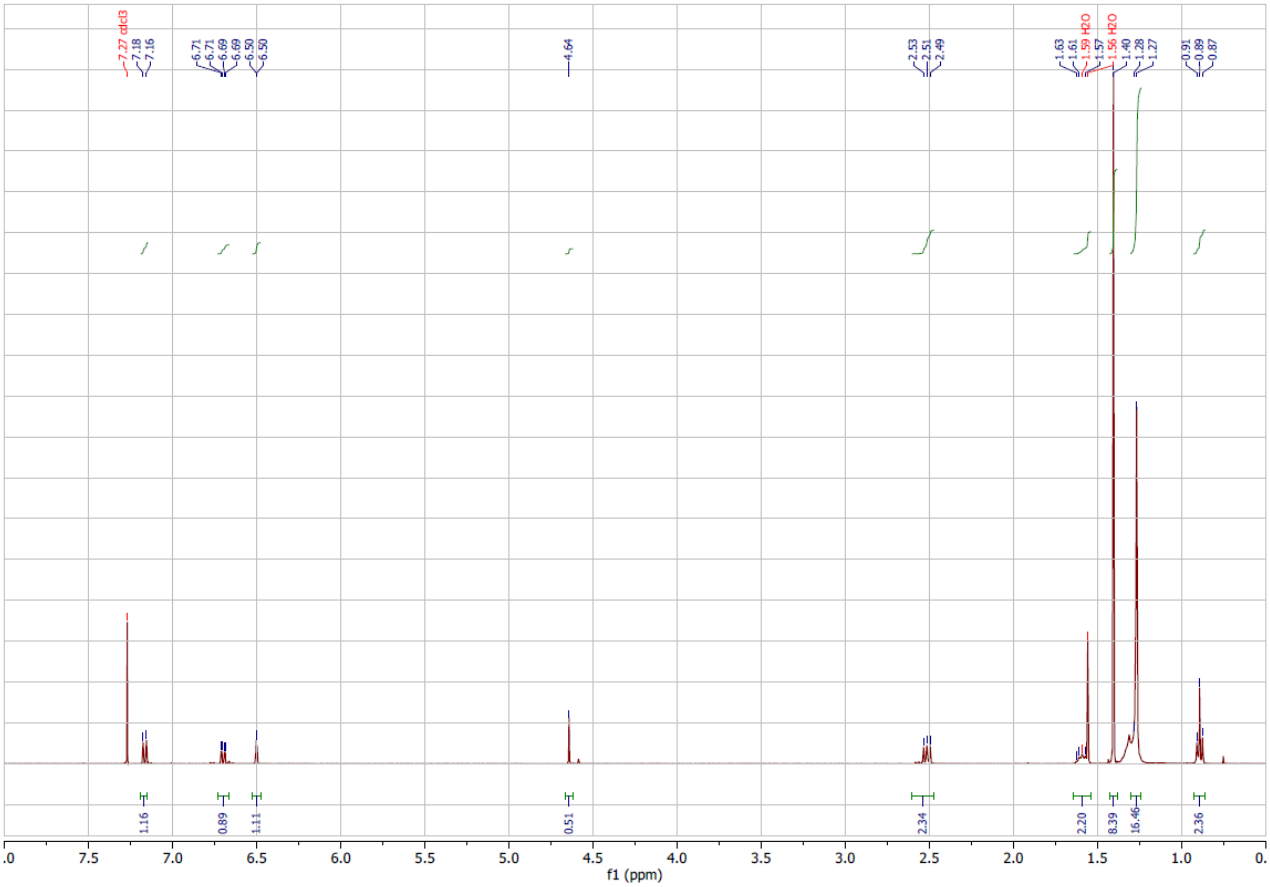

Fig. S1. ^{1}H NMR spectrum of TBC in deuterated chloroform.

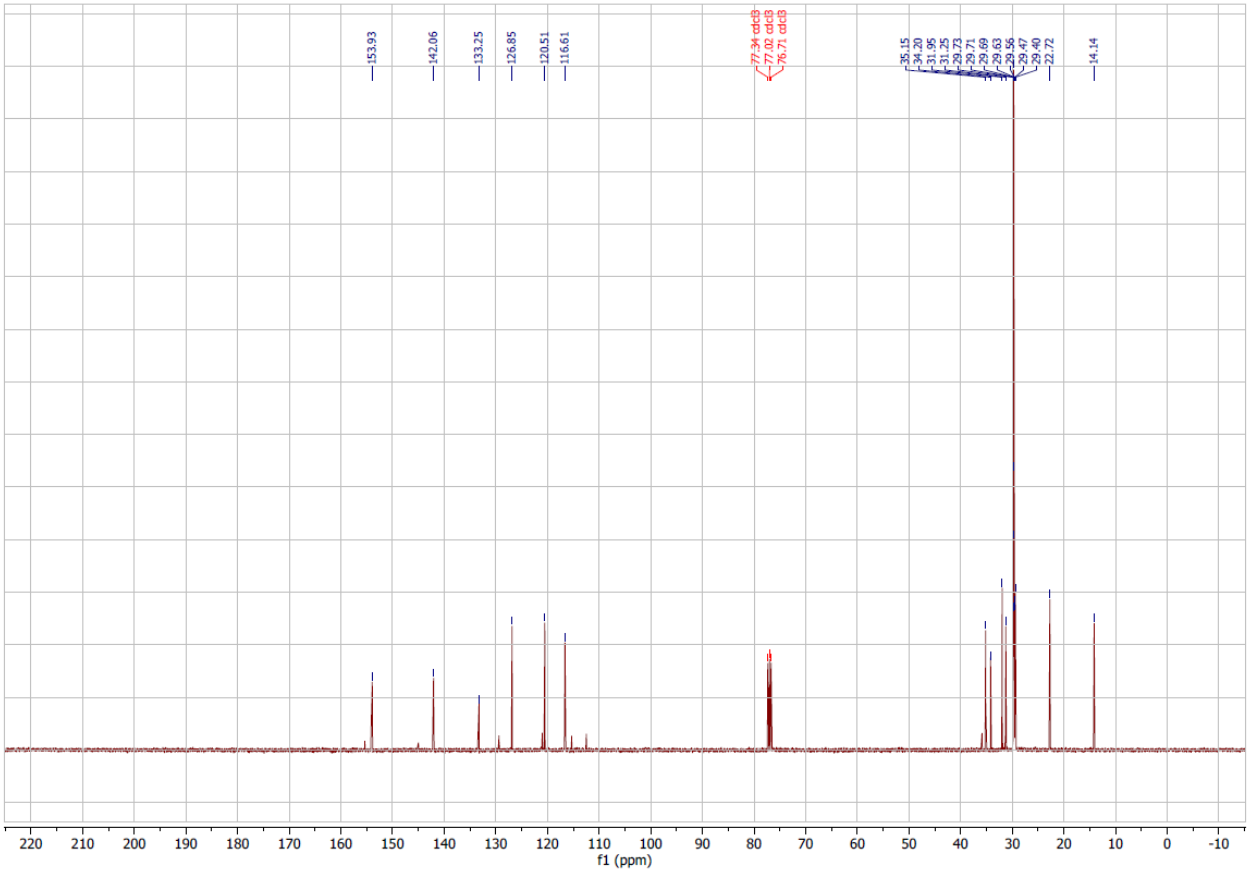

Fig. S2. ^{13}C NMR spectrum of TBC in deuterated chloroform.

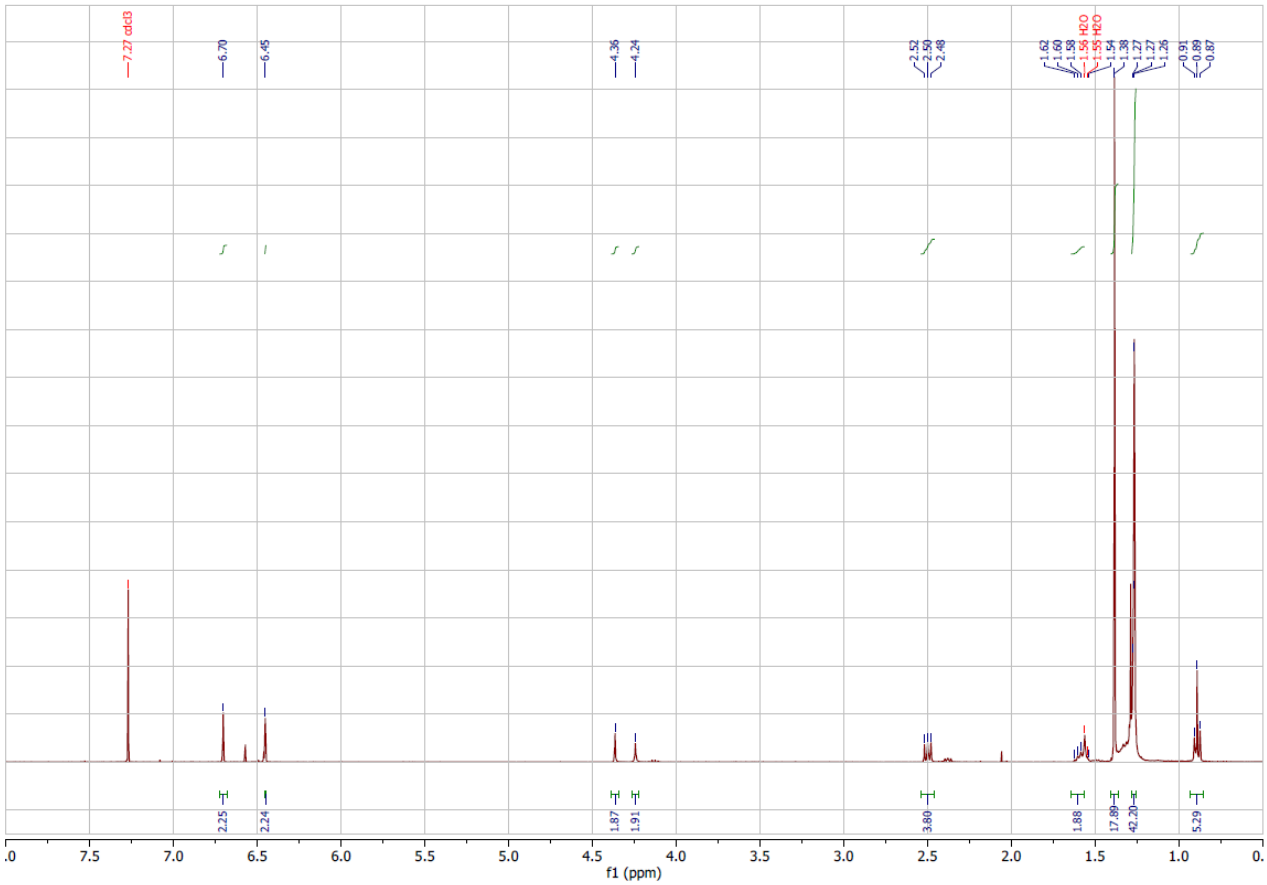

Fig. S3. ^{1}H NMR spectrum of TB(OH)C in deuterated chloroform.

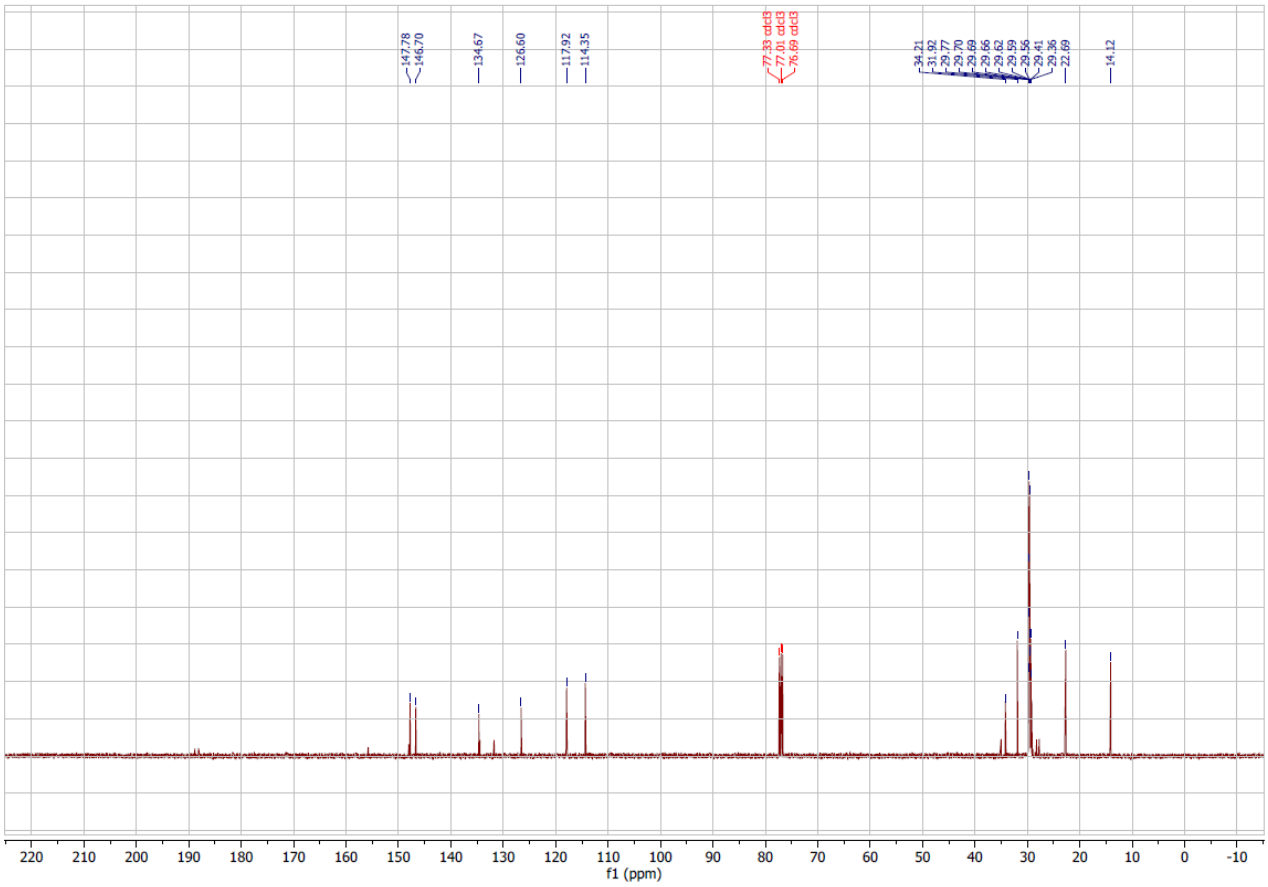

Fig. S4. ^{13}C NMR spectrum of TB(OH)C in deuterated chloroform.

S2. CMC determinations

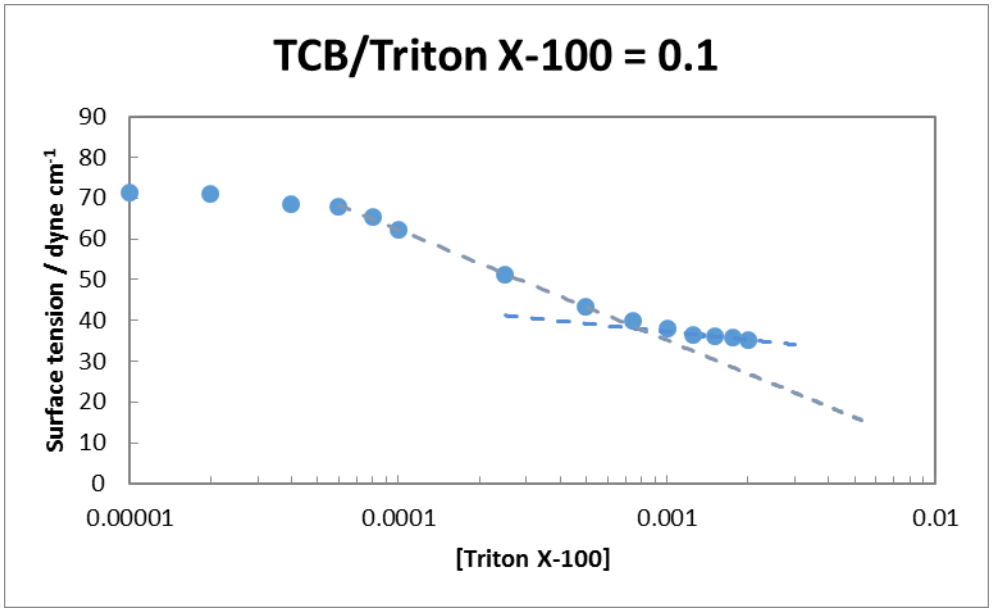

Fig. S5. Representative determination of the CMC of TBC/Triton X-100 micelles. The surface tension values (dyne cm^{-1}) were plotted against the decimal logarithm of the molar concentration of the Triton X-100, varied in the interval 1.00×10^{-5} – 2.00×10^{-3} M, in order to evaluate the relevant CMC as the point where the baseline of minimal surface tension and the slope where surface tension shows linear decline intersect.

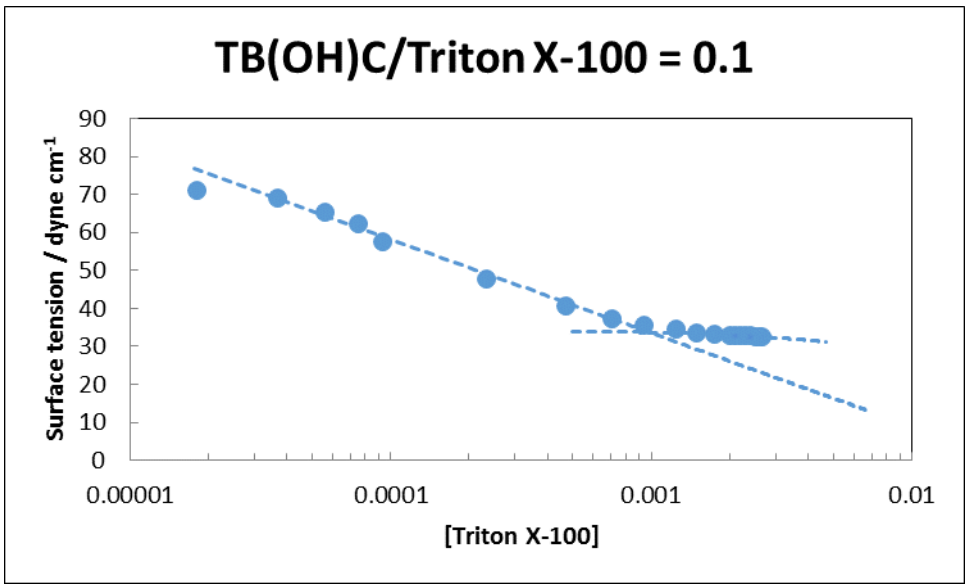

Fig. S6. Representative determination of the CMC of TB(OH)C/Triton X-100 micelles. The surface tension values (dyne cm^{-1}) were plotted against the decimal logarithm of the molar concentration of

the Triton X-100, varied in the interval 1.80×10^{-5} – 2.67×10^{-3} M, in order to evaluate the relevant CMC as the point where the baseline of minimal surface tension and the slope where surface tension shows linear decline intersect.

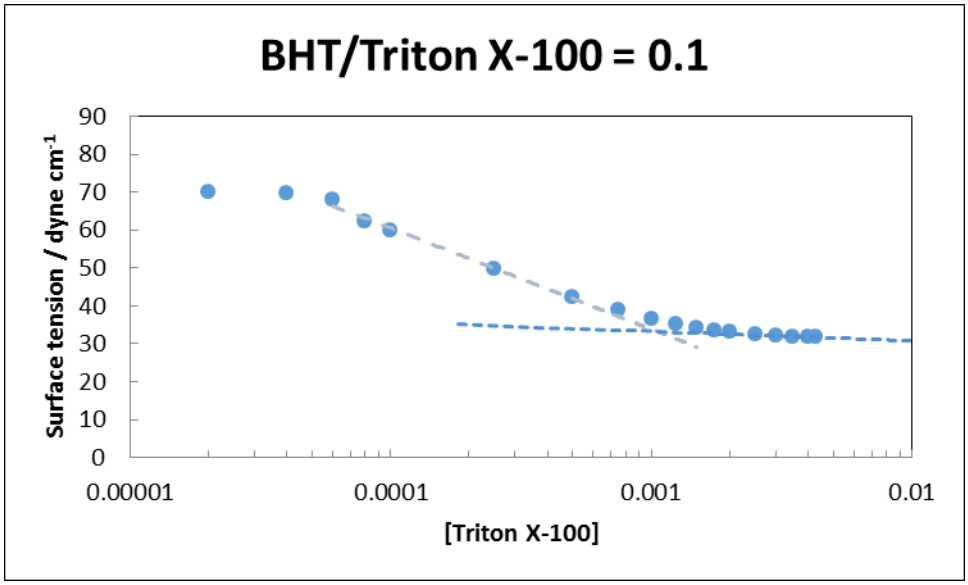

Fig. S7. Representative determination of the CMC of BHT/Triton X-100 micelles. The surface tension values (dyne cm^{-1}) were plotted against the decimal logarithm of the molar concentration of the Triton X-100, varied in the interval 2.00×10^{-5} – 4.28×10^{-3} M, in order to evaluate the relevant CMC as the point where the baseline of minimal surface tension and the slope where surface tension shows linear decline intersect.

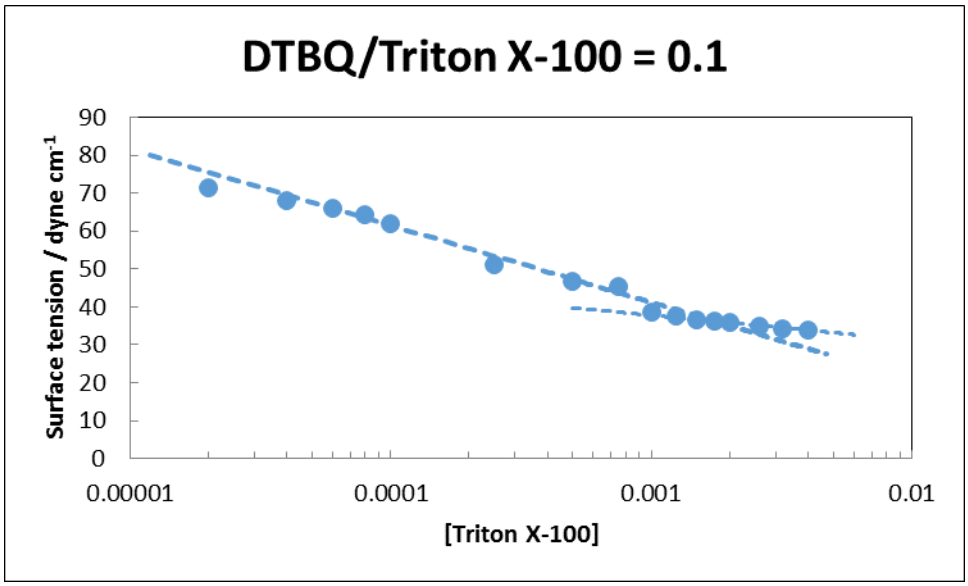

Fig. S8. Representative determination of the CMC of DTBQ/Triton X-100 micelles. The surface tension values (dyne cm^{-1}) were plotted against the decimal logarithm of the molar concentration of the Triton X-100, varied in the interval 2.00×10^{-5} – 4.00×10^{-3} M, in order to evaluate the relevant CMC as the point where the baseline of minimal surface tension and the slope where surface tension shows linear decline intersect.

S3. Determination of aggregation number

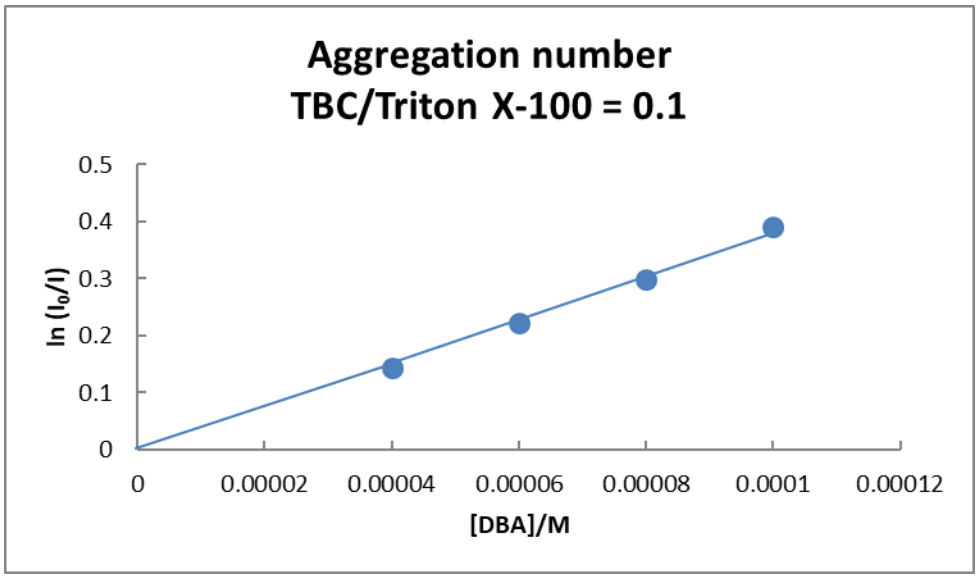

Fig. S9. Determination of the aggregation number of TBC/Triton X-100 micelles. The concentration of Triton X-100 was 2.00×10^{-2} M and pyrene 1.00×10^{-6} M. The concentration of the quencher N,N-dibutylaniline (DBA) varied in the interval 4.00×10^{-5} – 1.00×10^{-4} M.

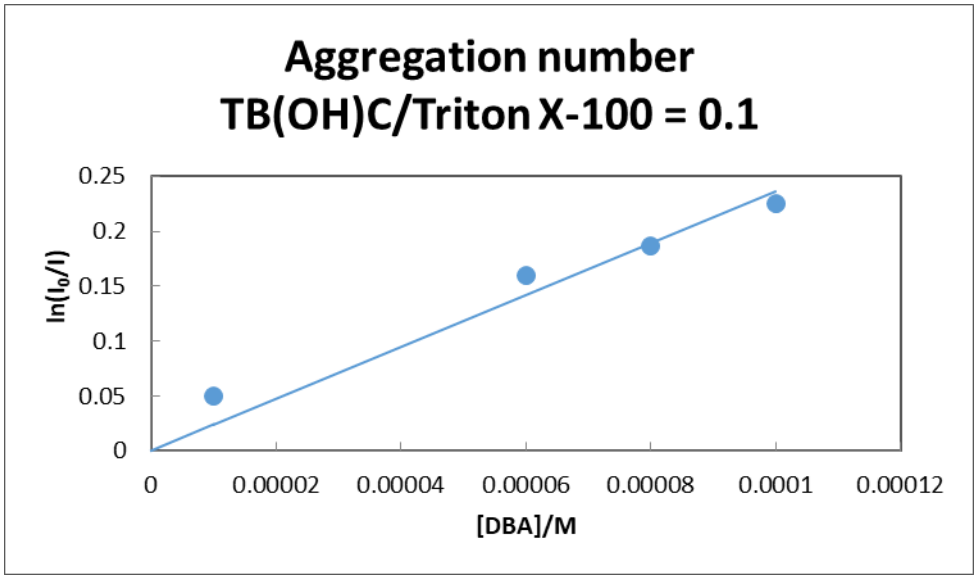

Fig. S10. Determination of the aggregation number of TB(OH)C/Triton X-100 micelles. The concentration of Triton X-100 was 2.00×10^{-2} M and pyrene 1.00×10^{-6} M. The concentration of the quencher N,N-dibutylaniline (DBA) varied in the interval 1.00×10^{-5} – 1.00×10^{-4} M.

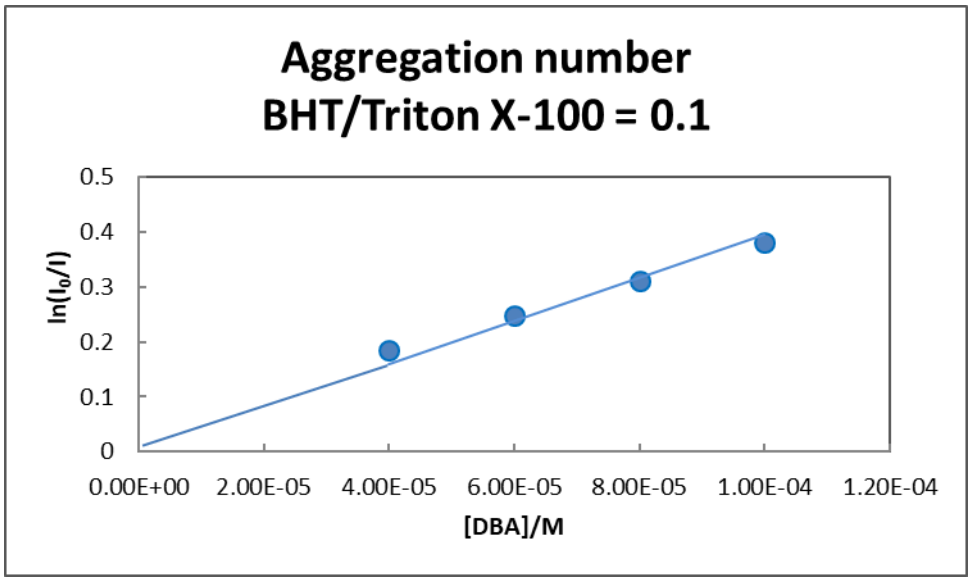

Fig. S11. Determination of the aggregation number of BHT/Triton X-100 micelles. The concentration of Triton X-100 was 2.00×10^{-2} M and pyrene 1.00×10^{-6} M. The concentration of the quencher N,N-dibutylaniline (DBA) varied in the interval 4.00×10^{-5} – 1.00×10^{-4} M.

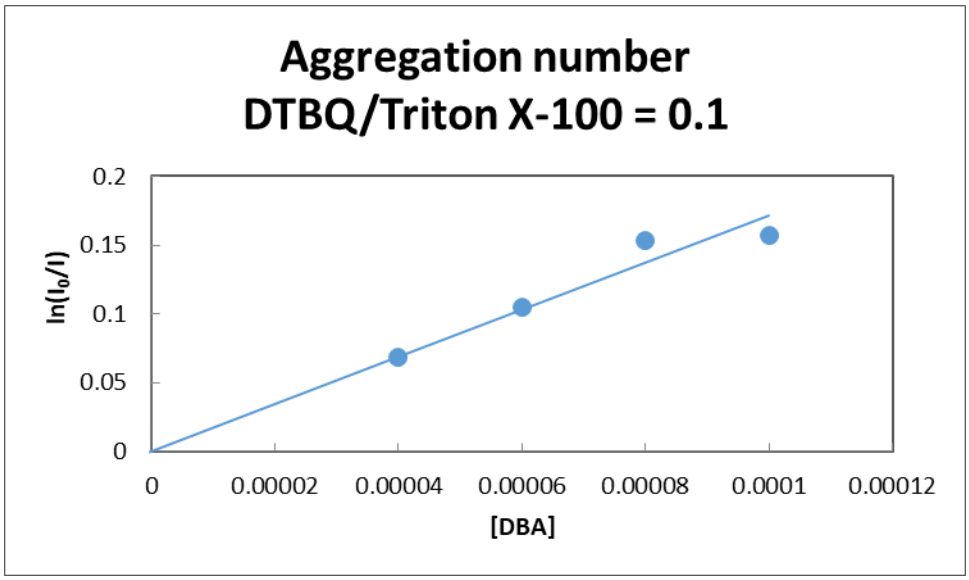

Fig. S12. Determination of the aggregation number of DTBQ/Triton X-100 micelles. The concentration of Triton X-100 was 2.00×10^{-2} M and pyrene 1.00×10^{-6} M. The concentration of the quencher N,N-dibutylaniline (DBA) varied in the interval 4.00×10^{-5} – 1.00×10^{-4} M.

S4. Microviscosity measurements

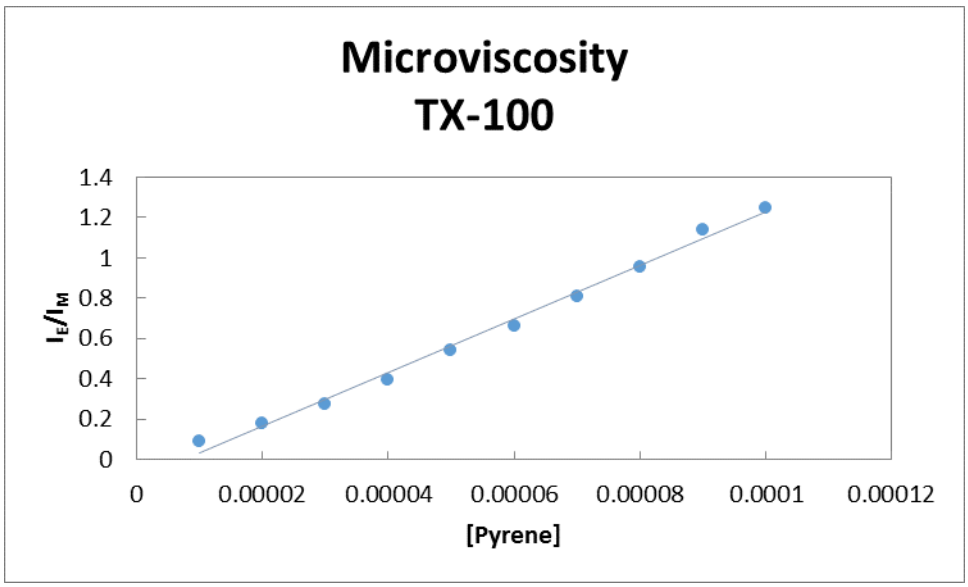

Fig. S13. Microviscosity of Triton X-100 micelles. at a constant Triton X-100 concentration of 2.00×10^{-3} M. Pyrene varied in the interval 1.00×10^{-5} – 1.00×10^{-4} M.

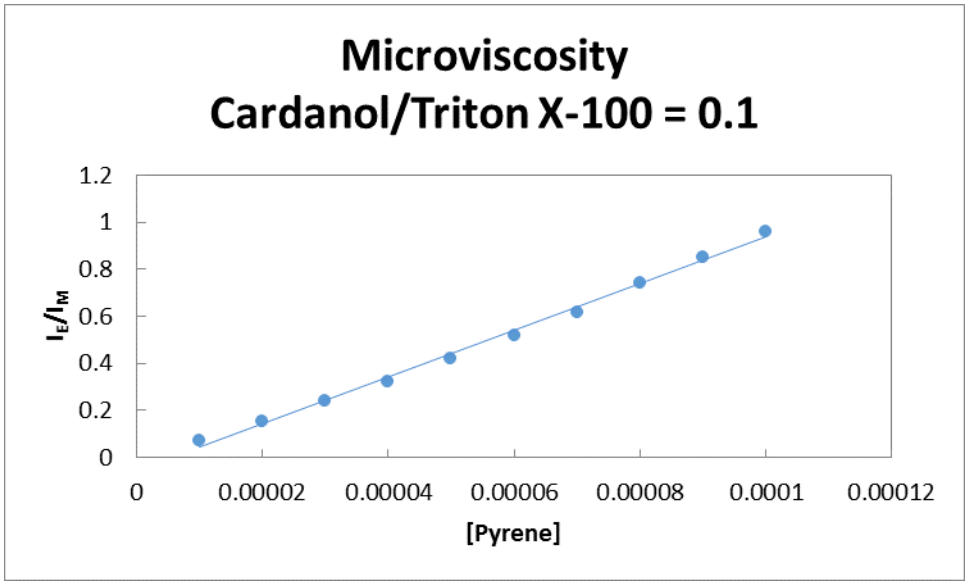

Fig. S14. Microviscosity of Cardanol/Triton X-100 micelles at a constant Triton X-100 concentration of 2.00×10^{-3} M. Pyrene varied in the interval 1.00×10^{-5} – 1.00×10^{-4} M.

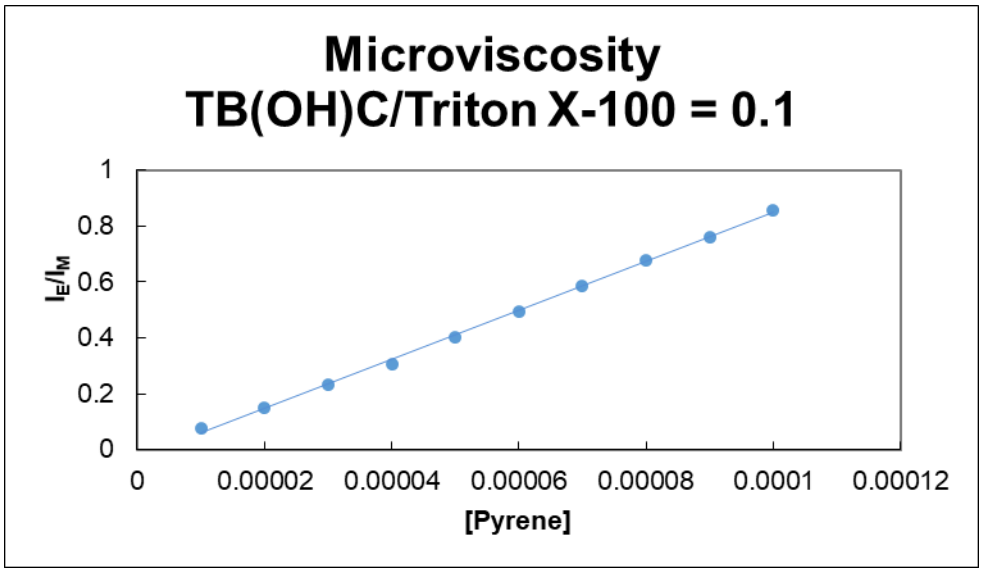

Fig. S15. Microviscosity of TBC/Triton X-100 micelles at a constant Triton X-100 concentration of 2.00×10^{-3} M. Pyrene varied in the interval 1.00×10^{-5} – 1.00×10^{-4} M.

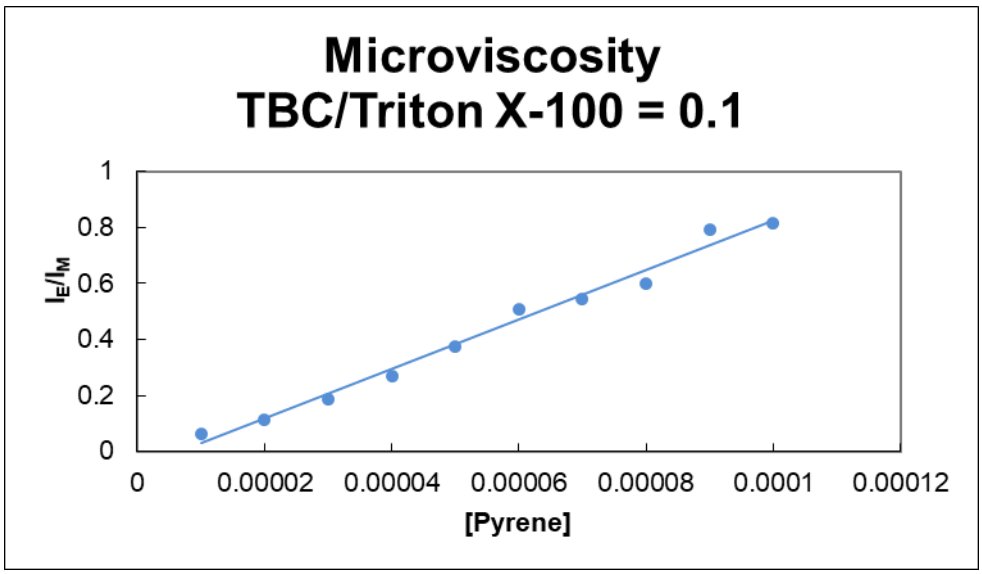

Fig. S16. Microviscosity of TB(OH)C/Triton X-100 micelles at a constant Triton X-100 concentration of 2.00×10^{-3} M. Pyrene varied in the interval 1.00×10^{-5} – 1.00×10^{-4} M.

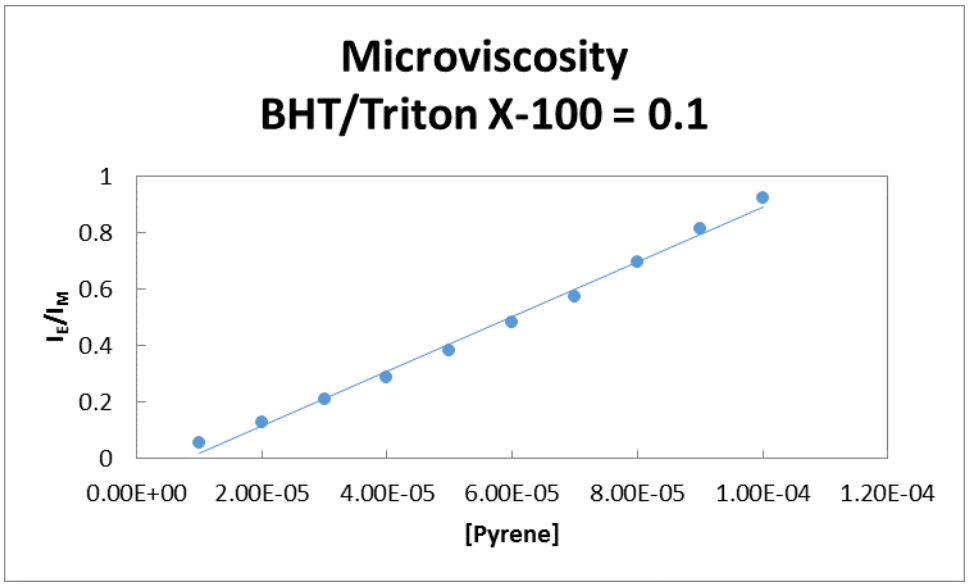

Fig. S17. Microviscosity of BHT/Triton X-100 micelles at a constant Triton X-100 concentration of 2.00×10^{-3} M. Pyrene varied in the interval 1.00×10^{-5} – 1.00×10^{-4} M.

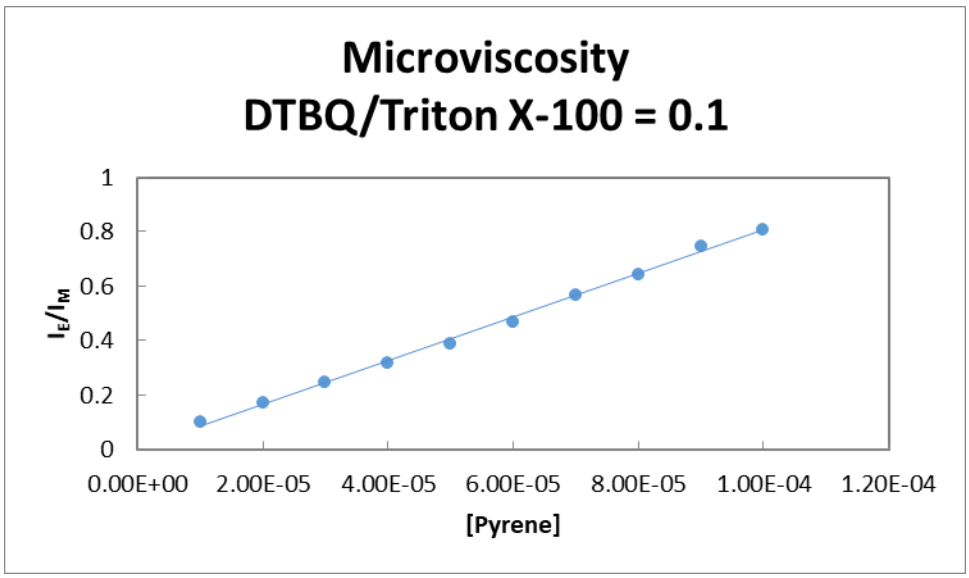

Fig. S18. Microviscosity of DTBQ/Triton X-100 micelles at a constant Triton X-100 concentration of 2.00×10^{-3} M. Pyrene varied in the interval 1.00×10^{-5} – 1.00×10^{-4} M.

S5. Fluorescence spectra of pyrene in the presence of DPPH

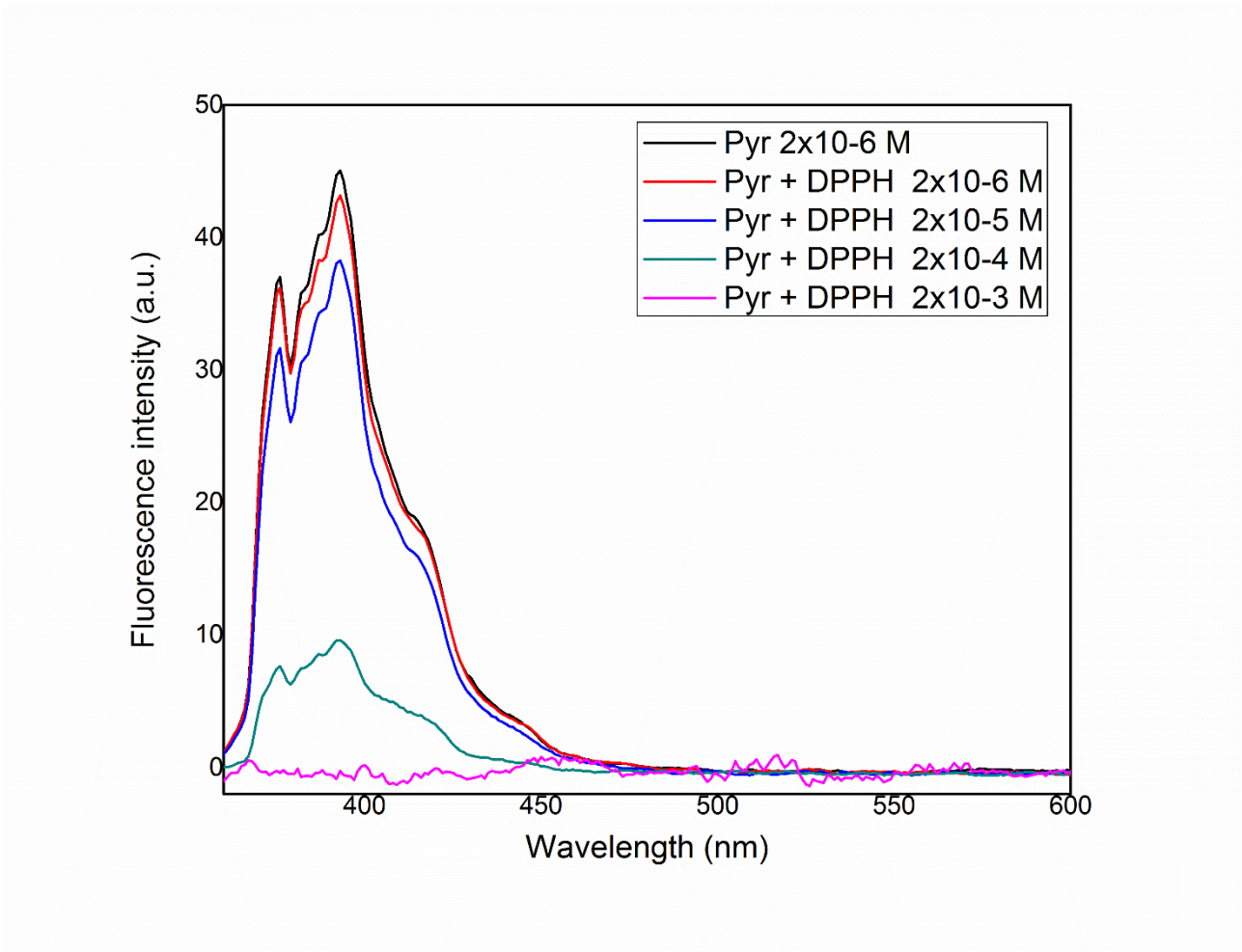

Fig. S19. Fluoresce spectra of pyrene in EtOH on addition of different amount of DPPH.

S6. Micelles Characterization: Dynamic Light Scattering (DLS)

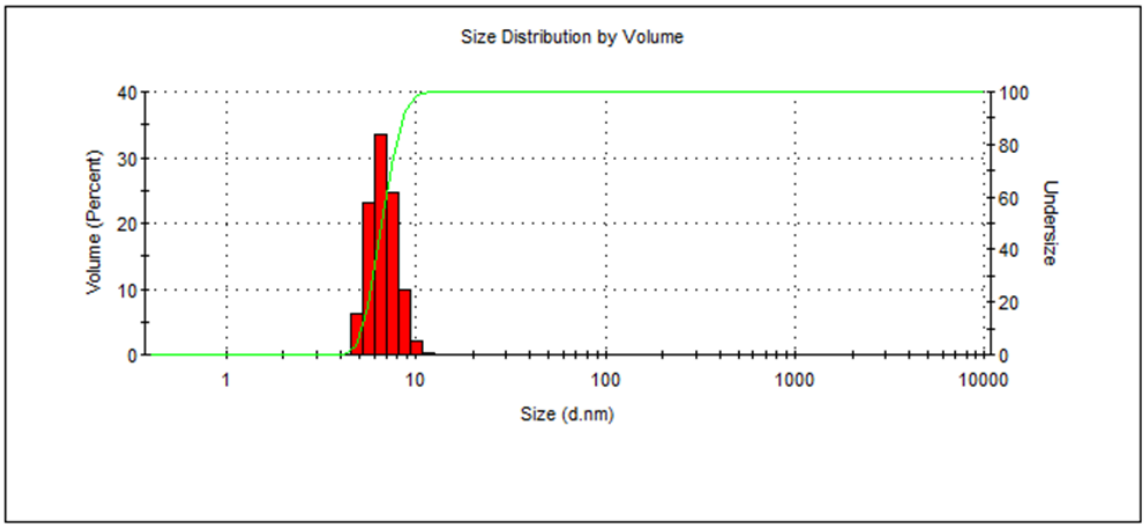

Fig. S20. Hydrodynamic diameter distribution of Triton X 100 1.00×10^{-3} M

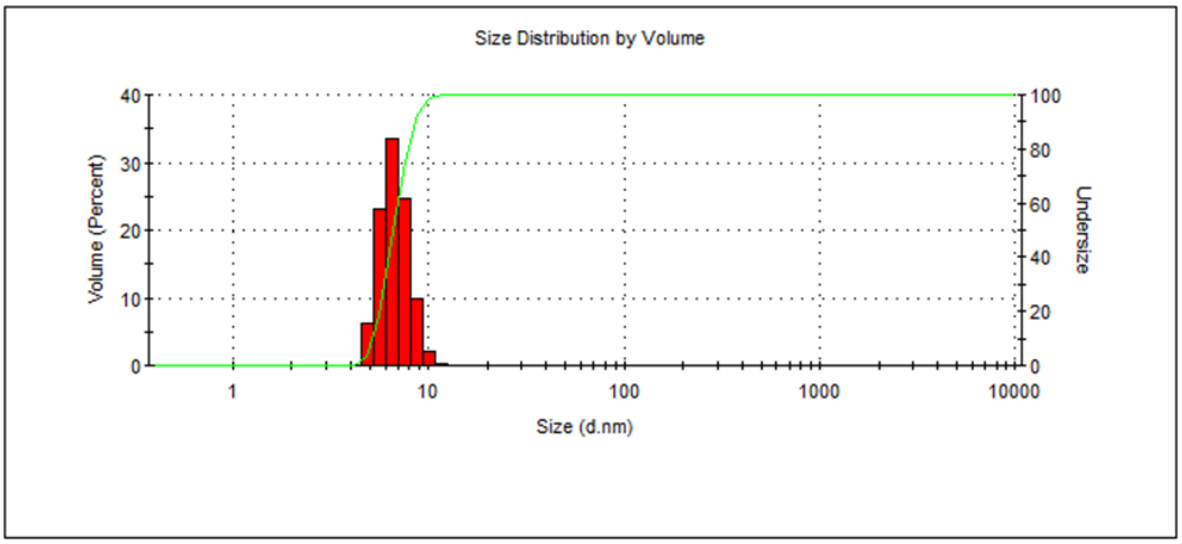

Fig. S21. Hydrodynamic diamater distribution TBC/Triton X 100 $1.00\times10^{-4}/1.00\times10^{-3}$ M

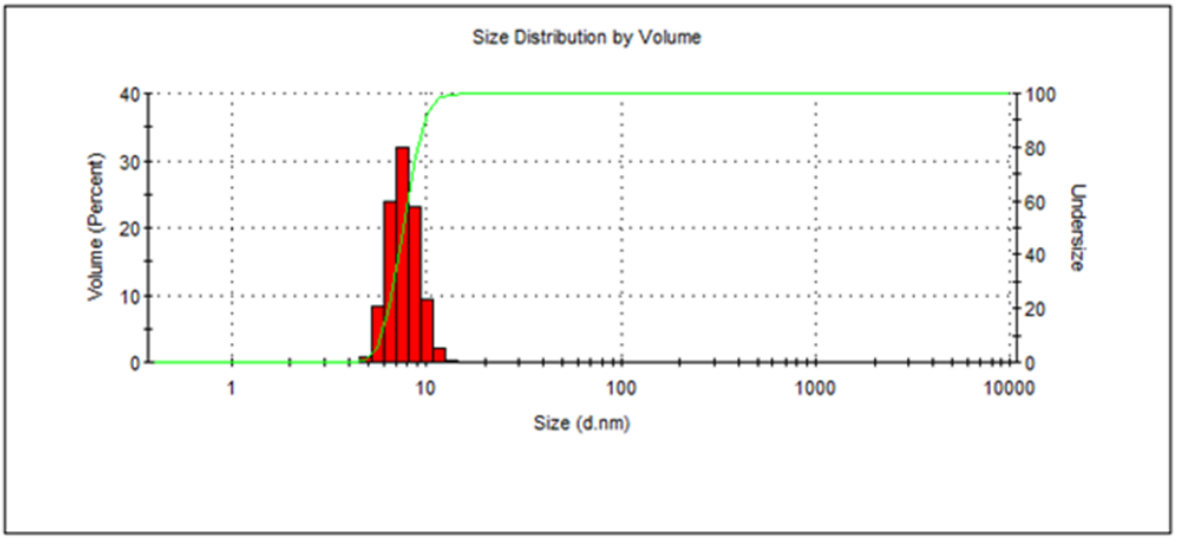

Fig. S22. Hydrodynamic diameter distribution TB(OH)C/Triton X 100 $1.00\times10^{-4}/1.00\times10^{-3}$ M

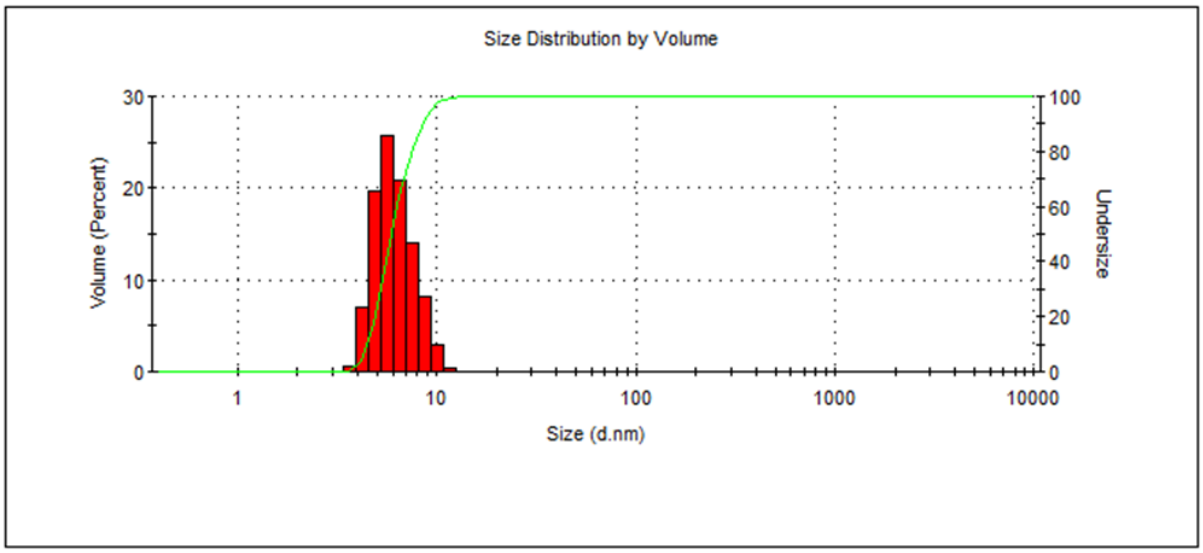

Fig. S23. Hydrodynamic diameter distribution BHT/Triton X 100 $1.00\times10^{-4}/1.00\times10^{-3}$ M

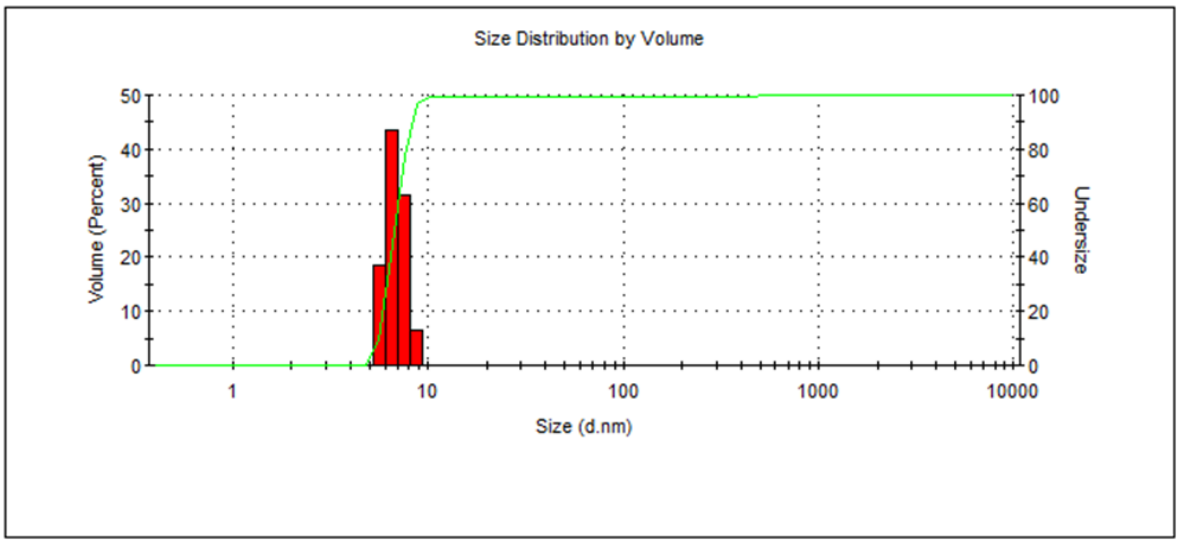

Fig. S24. Hydrodynamic diameter distribution DTBQ/Triton X 100 $1.00\times10^{-4}/1.00\times10^{-3}$ M

S7. UV-Vis spectra of DPPH• radical in different media

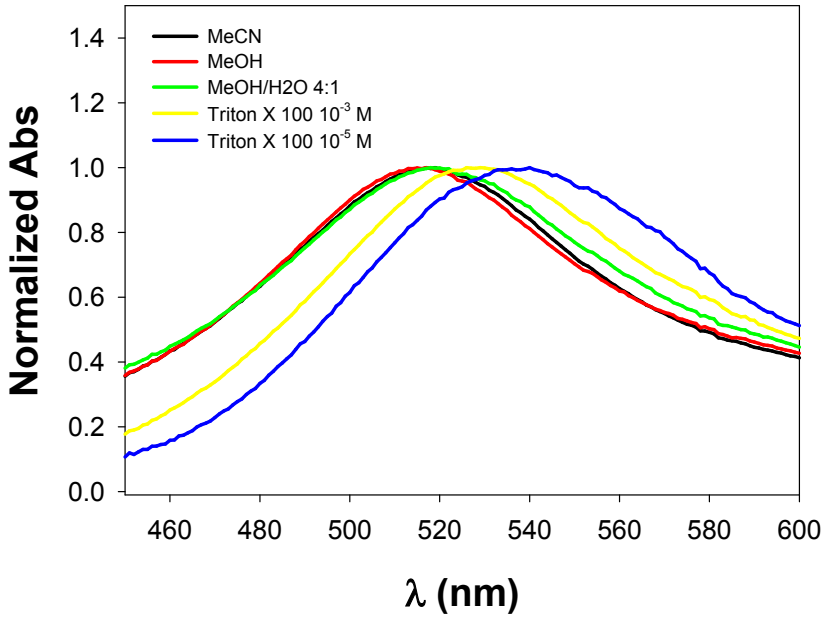

Fig. S25. Normalized absorption spectra of DPPH• 1.00×10^{-5} M in different media: acetonitrile (black line), methanol (red line), methanol/water 4:1 (green line), Triton X 100 1.00×10^{-3} M (yellow line), Triton X 100 1.00×10^{-5} M (blu line)

S8. Determination of DPPH scavenging

Table S1. Solvent effect on the reaction between DPPH• and monophenolic antioxidants.

Phenol	k_{DPPH} / $M^{-1}s^{-1}$			
	MeCN	**MeOH**	**MeOH+H_2O 20%**	**Triton**
TBC	0.7±0.3	0.7±0.2	1.3±0.3	5.0±0.9
BHT	0.21[a]	2.4[a]	4.0[a]	$(4.7\pm0.9)\times10^2$

a) From reference: Musialik, M.; Litwinienko, G. Scavenging of dpph• radicals by Vitamin E Is Accelerated by Its Partial Ionization: the Role of Sequential Proton Loss Electron Transfer. *Org. Lett.*, **2005**, *7*, 4951-4954.

S9. Kinetic analysis of DPPH• experiments

The absorbance at λ 517 nm was converted into the concentration of DPPH by using its molar extinction coefficient in Triton X-100 micelles of 6819 $M^{-1}cm^{-1}$.

In the case of monophenols (TBC and BHT), the kinetic traces were analyzed by the two following reactions:

$$PhOH + dpph^{\bullet} \underset{h}{\overset{k_{dpp}}{\rightleftharpoons}} PhO^{\bullet} + dpphH$$

$$2\ PhO^{\bullet} \xrightarrow{k_1} dimers$$

In the case of hydroquinone derivatives (TB(OH)C and DTBQ), after the reaction with DPPH•, a semiquinone radical is formed (QH• / $Q^{\bullet-}$) that reacts with oxygen forming superoxide, which exists in equilibrium with its protonated form. Superoxide can react with a second dpph• (k_5), disappear by disproportionation (k_3) or can deplete the hydroquinone antioxidant (k_4). Superoxide may also react with dpphH regenerating dpph•. In the last two cases, a stoichiometry of dpph• trapping < 1 is expected.

$$QH_2 + dpph^{\bullet} \xrightarrow{k_{dpph}} QH^{\bullet} + dpphH$$

$$QH^{\bullet} + O_2 \xrightarrow{k_2} Q + HOO^{\bullet}$$

$$HOO^{\bullet} \underset{}{\overset{pK_a}{\rightleftharpoons}} O_2^{\bullet-} + H^{+}$$

$$HOO^{\bullet} + O_2^{\bullet-} \xrightarrow{k_3} O_2 + H_2O_2$$

$$QH_2 + HOO^{\bullet} \xrightarrow{k_4} QH^{\bullet} + H_2O_2$$

$$dpphH + HOO^{\bullet} \xrightarrow{k_5} dpph^{\bullet} + H_2O_2$$

The value of k_2 is 1.6×10^6 $M^{-1}s^{-1}$ [Dohrmann, J. K.; Bergmann B. Equilibria and Rates of Redox Reactions Involving the 2-tert-Butyl-1,4-benzosemiquinone Radical in Aqueous Solution: An Investigation by Potentiometry, ESR, and Pulse Radiolysis. *J. Phys. Chem.* **1995**, *99*, 1218-1227], pK_a = 4.7 and $k_3 = 10^8$ $M^{-1}s^{-1}$ [Sawyer, D. T.; Valentine J. S. How super is superoxide? *Acc. Chem.*

Res., **1981**, *14*, 393-400], k_4 = 1.6 × 10^6 $M^{-1}s^{-1}$ [Valgimigli, L.; Amorati, R.; Fumo, M. G.; Di Labio, G. A.; Pedulli, G. F.; Ingold, K. U.; Pratt, D. A. The Unusual Reaction of Semiquinone Radicals with Molecular Oxygen. *J. Org. Chem*., **2008**, *73*, 1830-1841]. The concentration of O_2 in the sample is derived from the solublity of O_2 in water at 30°C in air: 2.36 × 10^{-4} M [Battino, R.; Rettich, T. R.; Tominaga, T. The Solubility of Oxygen and Ozone in Liquids. *J. Phys. Chem. Ref. Data*, **1983**, *12*, 163-178].

S10. Triton X-100 autoxidation

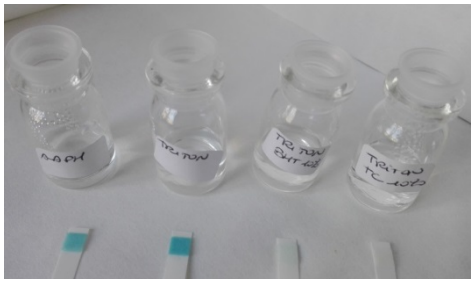

Fig. S26. Hydroperoxide formation was measured by using the QUANTOFIX® Peroxide test sticks (ferrous xylenol orange assay). In the presence of hydroperoxides, the test paper turns blue. In the samples containing either AAPH or AAPH + Triton X-100, the concentration of peroxides rapidly increases (the intensity of the blue crescent is more pronounced in the presence of Triton X-100).